BARRIER EFFECTS AND VOLUMETRIC ASSOCIATION IN DIFFUSION WEIGHTED ATTENUATED MAGNETIC RESONANCE IMAGING

Master's Thesis

Dániel Papp

Supervisor: ***Lajos R. Kozák, M.D, Ph.D.***
assistant professor
Mr Research Centre
Semmelweiss University
Budapest

Departmental Supervisor: ***Dávid Légrády, Ph.D.***
associate professor
Institute of Nuclear Techniques
Department Of Nuclear Techniques

Budapest University Of Technology and Economics

2012

ÖNÁLLÓSÁGI NYILATKOZAT

Declaration of independent work

Alulírott Papp Dániel, a Budapesti Műszaki Egyetem hallgatója kijelentem, hogy ezt a diplomatervet meg nem engedett segítség nélkül, saját magam készítettem, és a diplomatervben csak a megadott forrásokat használtam fel. Minden olyan részt, amelyet szó szerint vagy azonos értelemben, de átfogalmazva más forrásból átvettem, egyértelműen a forrás megadásával megjelöltem.

Budapest, 2012. 05. 25

_____

Kivonat

A diffúzió-súlyozott mágneses rezonancia képalkotás segítségével információ nyerhető a vizsgált minta, jellemzően az agy, vízkompartmentjeinek lokális diffuzibilitásáról, illetve a diffúziós irányok valószínűségi eloszlásáról. Az így nyert információ jól jellemzi a vizsgált rendszer strukturális felépítését, és integritását. A kapott információ értelmezése bizonyos szempontok szerint a mai napig nyitott kérdés.

Ilyen kérdés a b paraméterrel jellemzett, vizsgálni kívánt diffúziós sebesség és a jelintenzitás kapcsolata. A szokásos irodalmi értelmezésben a különböző b értékekénél mérhető jelintenzitás mono-, lasabb diffúzió, azaz magasabb b értékek figyelembe vételével pedig biexponenciális függvény szerint változik. Ezen biexponenciális viselkedés egy gyors és egy lassú komponensre osztja a jelet, és ezen jelkomponenseket a sejten belüli és a sejten kívüli vízterekkel szokás azonosítani.

Ez az azonosítás azonban nem teljes körűen elfogadott. Több bizonyíték is utal arra, hogy egy vízterű kompartmentekben is előfordulhat biexponenciális jeleloszlás, faleffektusok következtében.

Diplomamunkám során megvizsgáltam a jelintenzitás és a b érték közöti összefüggést egy klinikai scanneren, különféle összeállításokban. Megvizsgáltam a falhatást makroszkopikus és mikroszkopikus fantomok esetében, és kimutattam, hogy egy áthatolhatatlan fal hatására egy víztérben is kialakul egy nem monoexponenciális jel.

Megvizsgáltam a jel viselkedését egy kétkomponensű rendszerben, vörösvértest-szuszpenzióban. Eredményeim alapján kijelenthetem, hogy az intra-, és extracelluláris komponensek aránya hatással van a jelre.

Végeztem méréseket egy emberi agyban is. Megállapítottam, hogy a jel b-függése eltérő az agy különböző fehér és szürkeállományi területein. Az alkotott kép minőségéről megállapítottam, hogy erőteljesen függ a b értéktől.

Abstract

Diffusion-weighted magnetic resonance imaging is a tool for extracting structural and integrity information from the investigated compartment, usually the brain. This is done by measuring the local diffusibility of water, and the probability distribution of diffusion directions. The precise interpretation of obtained data is still an open question in many regards.

One such question is the relation between the measured signal intensity, and the investigated diffusion speed. In the general literary interpretation, the signal behaves exponentially with regards to the diffusion speed parameter, b. On fast diffusion speeds, corresponding to low b values. the signal is monoexponential. When measuring with high b values of up to 5000 s/mm^2, that correspond to low diffusion speeds, a second signal component arises, leading to a biexponential diffusion. The two signal components are associated with extra-, and intracellular water compartments.

This association carries in it a priori assumptions, and is thus not accepted by all researchers in the field. Biexponential signal behaviour has also been observed in single compartment systems, due to barrier effects.

In my master's thesis, I explored the connection between signal intensity and diffusion speed in a clinical scanner. I investigated barrier effects in micro-, and macroscopic phantoms, and found that the presence of an impenetrable barrier influences the non-monoexponentiality of the signal.

I investigated the signal behaviour in a two compartment system of red blood cells in saline solution. The ratio of intra-, and extracellular water has an effect on the signal behaviour.

Conducting measurements on a human brain, I found that the b-dependent signal intensity differs in grey and white matter. The quantification of structural information, the fractional anisotropy, also changes with the b value.

Table of Contents

Chapter I: introduction

Magnetic resonance imaging is a topographical, three dimensional, non-invasive imaging method based on a resonance phenomenon. Its subset, diffusion-weighted, or diffusion-attenuated imaging can return structural information by measuring the diffusibility, both in speed and probability distribution, of water in the investigated tissue, generally the brain.

In clinical practice, only one diffusion speed is measured. The diffusion speed is characterized by the b value, a composite of all pulse parameters. The higher the b value, the lower the investigated diffusion speed. For everyday clinical use, b=800-1200 s/mm^2. If more than b value is used to measure diffusion, the there will be an association between the intensity of the measured signal and the diffusion speed. On b values of less than 3000 s/mm2, this function is monoexponential. When measuring with b of up to 5000 s/mm^2, a second signal component arises, leading to a biexponential signal behaviour.

Based on phantom and in vivo measurements, these two signal components are generally associated with extra-, and intracellular water compartments for the fast and slow signal, respectively. This association, however, carries within it an a priori assumption regarding the origin of the signal.

New research, as detailed in Chapter V, shows that biexponential signal can arise in a single compartment due to the interaction of excited spins with the wall of the compartments. This is called the barrier effect. In my master's thesis, I aimed to find out if this effect can arise in micro and macroscopic systems when measured with a standard clinical scanner.

For my master's thesis, I also investigated the relation between intra and extracellular water compartmentalisation and the signal component behaviour, using saline solution of red blood cells.

The effect of multi-b measurements on fractional anisotropy maps of the human brain, as well as signal intensity in certain parts of the brain, was investigated as well.

The aim of my master's thesis is not to deliver a definitive answer about what causes the biexponential signal behaviour, but to demonstrate, that in a 3T clinical scanner, a non-monoexponential signal behaviour can arise from both volumetric association and barrier effects.

Chapter II: The physics of magnetic resonance imaging

II.1: The magnetic moment

Magnetic resonance imaging (henceforth: MRI) is based on a quantum mechanical property of all nuclei, the spin, or angular momentum, represented by $\vec{I}$. Spin is best visualized as the rotation of the particle along its own axis. The absolute value of spin as a vector value is derived from the spin quantum number, represented by I, in the following way [1]:

$$\left|\vec{I}\right| = \hbar\sqrt{I(I+1)} \tag{II.1}$$

Protons and neutrons, the particles that form a nucleus both have an absolute spin of ±1/2. It does not follow, however, that the spin of a nucleus is the sum of the spins of its protons and neutrons. Protons and neutrons have a tendency to form pairs in the nucleus. This results in nuclei having less observable spin than what the number of neutrons or protons would suggest. The spin of nuclei of the elements most abundant in the human body displayed in Table I:

Nucleus	Spin	Approx. atomic percentage in human body
^{1}H	+1/2	63%
^{12}C	0	12%
^{13}C	-1/2	0%
^{14}N	+1	0,58%
^{15}N	-1/2	0%
^{16}O	0	24%
^{17}O	5/2	0%
^{19}F	+1/2	0,0012%

Table 1: Spin values in the human body

As evidenced by Table 1, most methods relying on spins to image the human body will be using the ^{1}H nucleus. Coupled to the spin is another property, the nuclear magnetic dipole moment:

$$\bar{\mu} = \gamma\bar{I} \tag{II.2}$$

$$\left|\bar{\mu}\right| = \mu = \gamma\hbar\sqrt{I(I+1)} \tag{II.3}$$

The dipole moment is a vector value observable when the spin is placed in an external magnetic filed. The coupling characterised by the γ gyromagnetic ratio. For hydrogen, γ is 42.58 MHz/T.

In a magnetic field, a nucleus with a non-zero **μ**, thus a non-zero spin, will behave like a rotating magnet, or a current loop. The axis of this rotation will be varying on many factors, but the vector component that is parallel to the external magnetic field can be described easily. The conventional notation holds that the vector of the external field points into the z direction:

$$\overline{B_0} = B_0 \bar{z}I \tag{II.4}$$

Since **μ** is a quantum mechanic property, its z component can only take distinct values:

$$\mu_z = m_I \hbar \gamma \tag{II.5}$$

where m_I is another quantum number, the magnetic quantum number. This property of the nucleus can have the following 2I+1 discreet values [1]:

$$m_I = -I, -I+1, ...0, ...I-1, I \tag{II.6}$$

II.2.: Spin distribution and resonance

A discreet number of states implies that there is a property of the nucleus that changes with these states. In an extant external magnetic field, this property is energy.

Modelling the spin of ^1H with a bar magnet, we can derive that its energy will only be affected by the magnetic field if the angle between its axis, **μ**, and $\mathbf{B_0}$, is not zero. With m_I values of ±1/2, this hold true, since we can calculate the angle between the two vectors via the following equation[2]:

$$\theta = \cos^{-1}\left[\frac{\mu_z}{\mu}\right] = \cos^{-1}\left[\frac{m_I}{\sqrt{I(I+1)}}\right] \tag{II.7}$$

$$\theta = 54{,}77^\circ$$

Since this angle is not zero, it follows that there will be two distinct orientations, and thus, two distinct energy states. The orientation is either described as "pointing upward", or parallel with the magnetic field, or antiparallel, or "pointing downward", as illustrated on figure II.1:

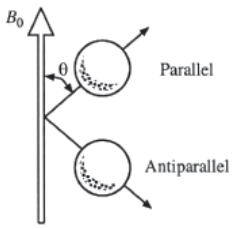

Figure II.1: Parallel and anti, parallel spin orientation [2]

The energy difference between the two states can be calculated in the following way[1]:

$$E = -\mu \cdot B_0 = -\gamma \hbar m_I B_0 \tag{II.8}$$

$$E_\uparrow = -\gamma \hbar B_0/2 \qquad E_\downarrow = \gamma \hbar B_0/2 \tag{II.9}$$

$$\Delta E = E_\uparrow - E_\downarrow = \hbar \gamma B_0 \tag{II.10}$$

These two energy states have a different population under normal circumstances, determined by the Boltzmann distribution, depending on the absolute temperature [2]:

$$N_\uparrow / N_\downarrow = e^{\frac{\Delta E}{kT}} \tag{II.11}$$

Solving equation II.11 for room temperature, where $\Delta E << kT$, the difference in the population of these two energy states can be calculated:

$$N_\uparrow - N_\downarrow \approx N \frac{\gamma \hbar B_0}{2kT} \tag{II.12}$$

It follows from equation II.12 that there is an excess number of spins on the lower energy level. However, when these spins absorb photons of exactly ΔE energy, they will enter the higher energy state. This energy selective excitation is the basis of magnetic resonance. The frequency of the absorbed photons can be calculated via Planck's equation:

$$\Delta E = \hbar \varpi = \hbar \gamma B_0 \qquad \varpi = \gamma B_0 \tag{II.13}$$

As can be gained from equation II.13, the resonance frequency is dependent on the magnetic field. Thus, by changing the magnetic field, the resonance frequency can be changed. This effect forms the basis of three-dimensional imaging in MRI.

II.3: The motion of the magnetic moment

To better understand the effects of the resonance, the dynamic behaviour of magnetic moments in an extant magnetic field must be described. A magnetic moment visualized as a bar magnet will experience torque in a magnetic field.

$$\bar{N} = \bar{\mu} \times \bar{B} \tag{II.14}$$

Since torque is defined as the time derivative of angular momentum, it follows for equations II.2 and II.14 that [1]:

$$d\bar{\mu} / dt = \bar{\mu} \times \bar{B} \gamma \tag{II.15}$$

The solution to equation II.15 is [1]:

$$\mu_x(t) = \mu_x(0)\cos(\varpi_0 t) + \mu_y(0)\sin(\varpi_0 t)$$
$$\mu_y(t) = \mu_y(0)\cos(\varpi_0 t) - \mu_x(0)\sin(\varpi_0 t) \qquad \text{(II.16)}$$
$$\mu_z(t) = \mu_z(0)$$

$$\mu_+(t) = \mu_x(t) + i\mu_y(t) = \mu_+(0)e^{-i\varpi_0 t} \qquad \text{(II.17)}$$

The behaviour described by equation II.17 is a precession, where the frequency of precession, also called Larmor frequency, is equal to $\omega_0=\gamma B_0$. This is the same frequency described by equation II.13. The magnetic moment rotates around the axis of B_0 the way a gyroscope tumbles around its own precession axis:

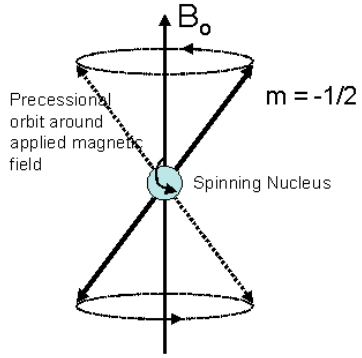

Figure II.2: Visualisation of precession [3]

The effect of a resonance excitation can be understood as flipping the axis of precession upward, so that it points in the same longitudinal direction (z), as the magnetic field. The energy required for the resonance phenomenon is in this description delivered via an oscillating magnetic field, denoted as $\overline{B}_1(t)$ that oscillates with the resonance frequency, and is perpendicular to the original field. Describing the movement of the magnetic moment is a standard coordinate system becomes complicated under such circumstances. Therefore, the usual method is to switch to a rotating frame of reference. If the rotational frequency of this frame of reference is ω, then the orthogonal unit vectors of e_x e_y e_z are transformed into the new unit vectors of e_x' e_y' e_z' in the folloqing way [1] [2]:

$$\overline{e_x}' = \overline{e_x}\cos(\varpi t) - \overline{e_y}\sin(\varpi t)$$
$$\overline{e_y}' = \overline{e_y}\cos(\varpi t) + \overline{e_x}\sin(\varpi t) \qquad \text{(II.18)}$$
$$\overline{e_z}' = \overline{e_z}$$

Since $\overline{B}_1(t)$ described above has only one nonzero component, $B_{1x} = B_1\cos(\varpi t)$, there will be a new effective magnetic field, where the equation of motion for the magnetic moment, described in the new coordinate system, is [1] [2]:

$$d\overline{\mu}/dt = \overline{\mu}\times\gamma\overline{B_{eff}} = \overline{\mu}\times\gamma\left(\overline{e_z}'\left(B_0 - \varpi/\gamma\right) + \overline{e_x}'\left(B_1/2\right)\right) \qquad \text{(II.19)}$$

The effect described by equation II.19 leads to a shift in the axis of precession from the z axis towards the x'-y' plane.

II.4: Free induction decay

Previously, the behaviour of a magnetic moment was described. Macroscopically, only the sum of these momenta, the bulk magnetisation, can be measured:

$$\overline{M}(r,t) = \frac{1}{V}\sum_{1}^{N}\overline{\mu}(r,t) \qquad \text{(II.20)}$$

The shift in the axis of precession can now be understood as introducing a measurable net magnetisation along the x'-y' plane into the system. This shift is caused by the $\overline{B}_1(t)$ field, and switching that field of results in the system returning to its base state, where the magnetisation is parallel to the B_0 field.

Free induction decay phenomenon describes the movement of the magnetisation vector after it has been completely shifted into the x-y plane. Such a rotation is called a 90°pulse, achieved by a radiofrequency excitation of $t = \pi/\gamma B_1$ duration. The magnetisation vector is perpendicular to the z axis after the field has been switched off, and returns to its original alignment in an oscillating and precessing motion:

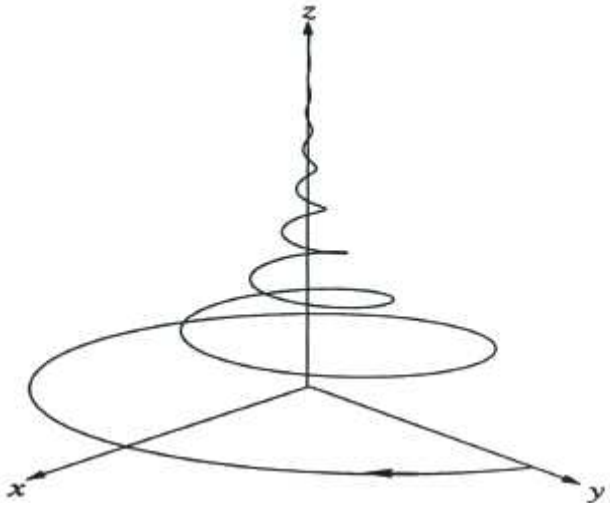

Figure II.3: The tip of the magnetisation vector during free induction decay [3]

II.5: The Bloch equations

The speed at witch the magnetisation reruns to its base state, also called relaxation, is dependent on several factors, and can be characterized by two time constants.

The magnetisation vector is generally separated into longitudinal magnetisation, parallel to the B_0 field, thus also z, and the transverse magnetisation, in the x'-y' plane.

Longitudinal magnetisation relaxes due to spin-lattice interactions. The higher energy state is an unstable equilibrium point, where an ideal spin without any interactions could remain indefinitely. However, any excited spin is surrounded by nonexcited spins, its so called lattice, with which it interacts. This lattice acts as a heat bath, and attempts to thermalise the excited spins, returning them to the stable equilibrium point of lower energy. The speed of this thermalisation is dependent on the strength of spin-lattice interaction. A tight lattice, like a solid will have a quick relaxation, while a loose lattice will have a slower relaxation. The time constant of spin-lattice relaxation is denoted as T_1, and defined as the time needed to reach 1-(1/e)≈63% of the original longitudinal magnetisation after the magnetisation vector has been flipped to the x'-y' plane by a 90°excitation.

While the loss of longitudinal magnetisation is a loss of energy, the loss of transverse magnetisation is a loss of phase coherence. Ideally, a packet of excited spins will have the same phase, or in other words, will travel as one group in the x'-y' plane. Spins in motion are however themselves sources of magnetic fields, as are surrounding electrons, and thus, every spin of this packet experiences a different field, and has a different phase. After a time, this phase decoherence leads to a loss of net magnetisation in the x'-y' plane. The time constant, T_2 is defined as the time it takes the transverse signal to diminish to 1/e≈37% of its original strength. The spins and electrons of the surroundings are not the only cause for field inhomogeneities. The original B_0 field is also never fully homogeneous. The net effect of intrinsic and external field inhomogeneities is defined with the time constant of T_2^*, calculated as $1/T_2^* = 1/T_2 + 1/T_{inh}$.

The dynamic behaviour of the transverse and longitudinal magnetisation is described by the principal equations of MRI, the Bloch-equations. After a simple 90°flip of the magnetisation into the x'-y' plane [1] [2]:

$$\begin{aligned} dM_z/dt &= \frac{M_0 - M_z}{T_1} \\ d\overline{M_\perp}/dt &= \gamma\overline{M_\perp} \times \overline{B_0} - \frac{\overline{M_\perp}}{T_2} \end{aligned} \qquad \text{(II.21)}$$

II.6: Basic pulse sequences

Using excitation of different angles and in different planes, diverse information can be extracted from a packet of spins.

In inversion recovery, or IR sequences, the longitudinal magnetisation if flipped in the opposite direction using a 180° pulse along the z axis. The longitudinal magnetisation thus starts as a negative value, and builds up back to its original strength, passing the zero point. A measurable component in the form of transverse magnetisation is introduced TI (inversion time) after the original z-axis 180°flip, in the form of a 90°rotation into the x'-y' plane. The net signal is governed by the diminishment and reappearance of the longitudinal magnetisation, and thus, by the T_1 time parameter. IR is an easy method to measure the T1 if a given tissue.

Spin echo (SE) sequences are used to measure T_2. As discussed, a spin packet will lose its coherence as it travels in the x'-y' plane. Some of the spins travel faster, some slower. This loss of coherence gradually weakens, and, when decoherence is total, destroys the signal. If. however, after a τ time, a 180°flip on the x'-y' plane is introduced, then the spins now travel in the opposite direction. This causes the fast spins to catch up with the slower ones, resulting in a gradual build-up of the signal. Once all spins catch up, they are once again one packet, and the signal strength is equal to the original. The catch-up occurs at TE=2τ echo time. Since the spins will now once again lose coherence, another 180°flip can be introduced, and such multiple flips are called a multiple echo sequence [4].

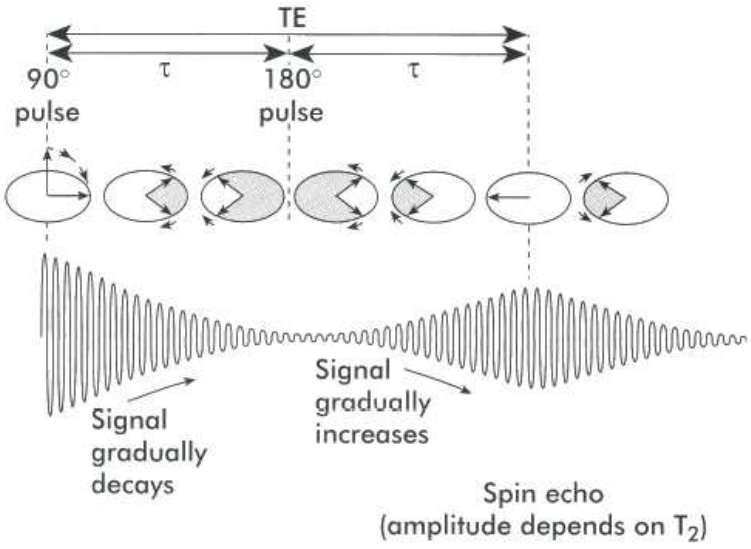

Figure II.4: Spin echo sequence [5]

T_2^* can be measured by gradient echo sequences. Here, dephasing is achieved by switching on a gradient that heavily alter phase, and thus quickly eliminates the signal by destroying coherence. If the same gradient is applied later in the opposite direction, the opposite effect is achieved, and the spins regain their coherence. Due to inhomogeneities in the external field, this rephasing is incomplete, leading to a signal loss governed by T_2^*

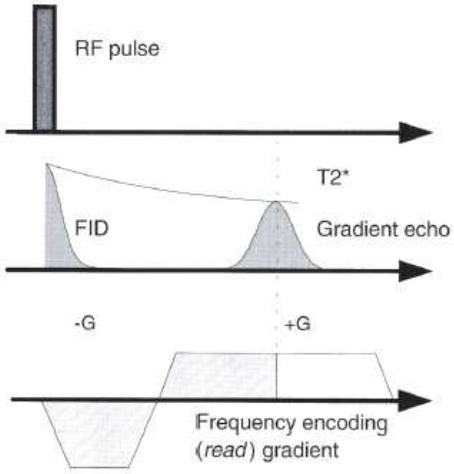

Figure II.5: Gradient echo achieved by the readout gradient [5]

Chapter III: MRI in practice

III.1: Instrumentation

The energy difference between the two energy states of excited and nonexcited spins is, as previously shown, dependant on the external magnetic field. The bigger the external field, the greater the difference, and thus, the greater the signal intensity. For this reason, clinical scanners have a strong B_0 external magnetic field ranging from 1T to 7T, with 3T machines being the most common. This external field is generated by a liquid helium cooled superconducting electromagnet of NTi or Nb_3Sn material [6].

Such a field will be inhomogeneous by its very design. These inhomogeneities are corrected using shimming, which done by using smaller, localized magnets, resistors, or magnetized iron elements. A shimmed magnetic field will be homogeneous to its eights-to-twelfth degree.

A totally homogeneous field will result in one resonance frequency over the whole sample. For three dimensional localisation this frequency must vary from place to place. This is done by introducing fields of known strength and direction, via the gradient coils. The gradients are linear, thus the field strength can be described as $B(r)=G(r)\cdot r$.

The localized spins have to be excited. Radiofrequency coils are requires to introduce photons of appropriate frequency into the sample, and thus cause excitation. After the excitation stops, the magnetisation will return to its base state, the time dependence governed by relaxations. The change in magnetisation generates current in the receiver coils, from which the signal is then formed. More than one receiver coil is needed for three dimensional localisation. The sensitive fields of these coils generally overlap, allowing the localisation to be encoded by the sensitivity of overlapping coils. This is the basis of sensitivity encoding, or SENSE.

III.2: Spatial localisation and k-space

For three dimensional image formation, only specific voxels can be excited and measured. The spoiling of a homogeneous field with select gradients introduces such a selection.

First, the measured slice, or z-oriented component of the sample must be selected. This is done by introducing a gradient field parallel to the B_0 field. The strength of the slice selection gradient is defined by the desired resonance frequency of ω, and the selected z slice:

$$z = (\varpi/\gamma - B_0)/G_{SS} \tag{III.1}$$

Ideally, a z slice could be infinitely thin with infinitely strong box function gradients. In reality, gradients are of finite strength, and are sloped, resulting in a general slice thickness of 1-2 mm. Fixing the z coordinate leaves the x-y plane to be localized, via a resonance frequency shift of Δω.

Localisation along the x-y plane, or $\bar{x}$ is referred to as phase and frequency encoding, and is in essence a Fourier transform. The solution of the Bloch-equations for transverse magnetisation, with relaxations ignored, yields the following complex form in the absence of gradients [1] [2]:

$$\bar{M_\perp}(\bar{x},t) = M_0(\bar{x})\exp(i\varpi_0 t) \tag{III.2}$$

Dependence on location is a result of the excitable spin density ρ being dependent on the location in most samples. When a gradient of G(τ) is switched on in the x-y plane for a t time, the solution to (II.21) changes:

$$\bar{M_\perp}(\bar{x},t) = M_0(\bar{x})\exp(i\varpi_0 t + \varphi(\bar{x},t)) = M_0(\bar{x})\exp(i\varpi_0 t)\cdot\exp(i\varphi(\bar{x},t)) \tag{III.3}$$

$$\varphi(\bar{x},t) = \int_0^t \Delta\varpi(\bar{x},\tau)d\tau = \int_0^t \gamma\Delta B(\bar{x},\tau)d\tau = \gamma\int_0^t G(\tau)d\tau\bar{x} = 2\pi\cdot\bar{k}(t)\bar{x} \tag{III.4}$$

$$k(t) = \gamma\Big/ 2\pi\int_0^t G(\tau)d\tau \tag{III.5}$$

$$\bar{M_\perp}(\bar{x},t) = M_0(\bar{x})\exp(i\varpi_0 t)\cdot\exp(i2\pi\bar{k}(t)\bar{x}) \tag{III.6}$$

The magnetisation described by equation III.6 generates a voltage in the receiver coil that will be proportional to the magnetisation. From this, the signal can be gained by removing the part caused by the known ω_0 component. Thus, the signal S(t) is a Fourier transform of the spin density ρ:

$$U(t) = c\cdot\int M_\perp(\bar{x},t)d\bar{x} = \int M_0(\bar{x})\exp(i\varpi_0 t)\cdot\exp(2\pi i\bar{k}(t)\bar{x})d\bar{x} \tag{III.7}$$

$$U(t) = c'\cdot\exp(i\varpi_0 t)\int\rho(\bar{x})\exp(2\pi i\bar{k}(t)\bar{x})d\bar{x} \tag{III.8}$$

$$S(t) = \exp(-i\varpi_0 t)U(t) = c''\int\rho(\bar{x})\exp(2\pi i\bar{k}(t)\bar{x})d\bar{x} \tag{III.9}$$

The integral in equation III.9 is a Fourier transformation. Thus, MRI is in essence a Fourier transform, with the signals phase and frequency information corresponding to the spatial location of the excited voxel. A k(t) vector in k-space corresponds to a spatial location in real space. The sampling of the phase-frequency encoding k space determines the spatial readout sequence, and thus the reconstruction algorithm for an image.

III.3: Sampling k-space

The order of magnitude for T_1 is 400 ms-1 s, while for T_2, its 40-200 ms. If in a 256×256×128 voxel volume, which is standard for MRI, each voxel is weighed once for T_1, the whole measurement would take 8400000 seconds, or roughly 97 days. Patients only tolerate the circumstances of an MRI measurement for upwards an hours, thus more than one voxel, more than one k-space point must be read out at one time. A readout pattern for a single excitation is called a trajectory in k-space. The form of a trajectory depends on gradients.

The simplest to visualize, and fastest trajectory is the so called EPI, or echo-planar imaging sequence. In essence, the k space is read out row after row, with readout directions flipping every column change. This is done by reversals of the gradient in the x direction, known as the frequency-encoding gradient. This will produce a series of gradient echoes, an echo train. The y directional, or phase-encoding gradient can be held constant. The sampled points are equidistant, which is very beneficial to image reconstruction, but due to the gradient echo, the signal strength is governed by T_2^*, necessitating a very quick readout. During our measurements, we used EPI sequences.

An equidistant readout requires boxcar form gradients. If, however, sinusoidal gradient behaviour, which is much easier to control, is used, then the readout trajectory will be a spiral on the k-space. This readout technique is not hindered by T_2^* relaxation, but due to the non-equidistant sampling of k-space, image reconstruction is very difficult.

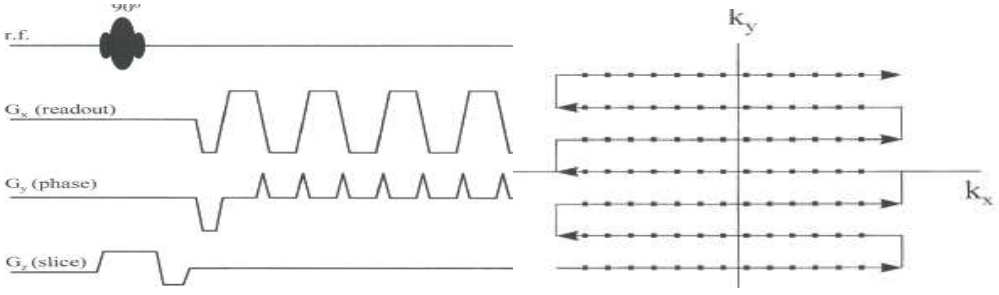

Figure III.1: EPI gradients and k-space sampling [5]

Chapter IV: Diffusion weighted imaging

IV.1: The physics of diffusion

Diffusion is in its broadest definition, the random movement of matter governed by either temperature, or a gradient in concentration. In MRI, we only consider the former definition, the so called molecular diffusion.

Molecular diffusion postulates that at any nonzero temperature, particles will move in a random walk manner with the average displacement dependent on the temperature, but the net displacement being zero. This random movement leads to a mixing of the particles, and is not to be confused with flux, which is an ordered net movement into one direction.

As previously noted, molecular diffusion is a random process, necessitating a statistical description. This is best done first in one dimension. If at t=0, there are N molecules in a single volume, and no molecules anywhere else, then the particle density function p(x,t) is described by the diffusion equation:

$$\frac{\partial \rho}{\partial t} = D\frac{\partial^2 \rho}{\partial^2 x} \qquad \text{(IV.1)}$$

D denotes the diffusion coefficient, which depends on temperature in the following way:

$$D = D_0 \exp(-E_A / RT) \qquad \text{(IV.2)}$$

D_0 is the diffusion coefficient at infinite temperature, while E_A is the activation energy of the process. At 25°C, the diffusion coefficient of water in an unrestricted space is $D \approx 2.27 \cdot 10^{-3} mm^2 s^{-1}$. [7].

The solution to equation IV.1 is a Gaussian function that describes the probability of any given particle being in the voxel x at the time of t:

$$\rho(x,t) = \frac{1}{\sqrt{4\pi D}} \exp(-x^2 / 4Dt) \qquad \text{(IV.3)}$$

In a more generalized form, this function describes the displacement probabilities during any given time, that is, the probability of any given voxel along the x avis containing a given number of molecules.

The Gaussian nature means that we can calculate the mean square displacement over a given time of Δ:

$$\left\langle x^2 \right\rangle = 2 \cdot D \cdot \Delta \qquad \text{(IV.4)}$$

With the previous equations, we assumed diffusion in one dimension. However, if there is no restriction in the medium, if the only equation governing the system is IV.1, then we can describe the behaviour in 3 dimensional systems the same way. In any given direction, said equation describes the behaviour, leading to a 3 dimensional Gaussian function. Representing the probability function with a colour code, we can represent the three dimensional function in two dimensions[8]:

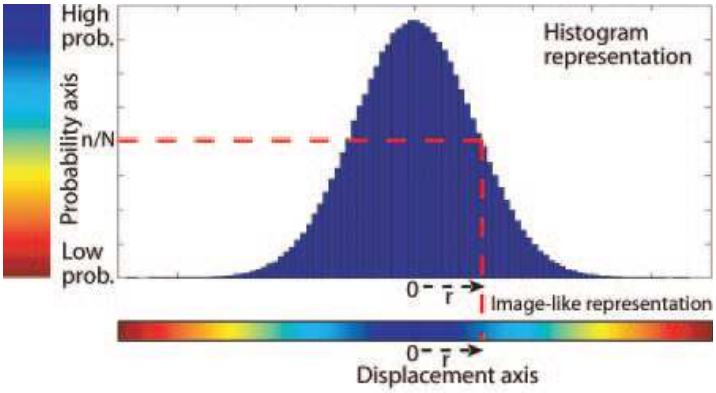

Figure IV.1: The displacement histogram[8]

Figure IV.1 shows the colour coding representation of equation IV.3 along a given r axis. The figure also assumes a histogram distribution, not a continuous one. Using the convention above, and applying it to three dimensions, we get:

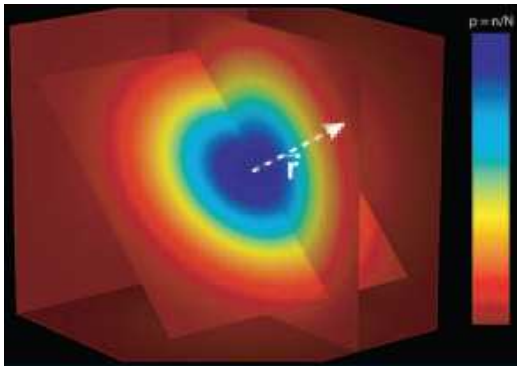

Figure IV.2: Three dimensional representation of displacement

Figure IV.2 shows the probability in an isotropic, three-dimensional space. The deeper the colour, the more particles diffuse to that voxel. The Gaussian diffusion along any axis results in a symmetrical profile, with the centre having the highest probability. Any imperfection and anisotropy in the system will alter the above described behaviour.

IV.2: Diffusion in biological tissue

In section IV.1, we only discussed the non-restricted diffusion of free water in a limitless space. This description is insufficient for biological systems. Tissue are usually not a homogeneous, but heterogeneous, and therefore restrict the movement of diffusing particles. Generally, the more heterogeneous the tissue, the higher the restriction, resulting in lower diffusion speeds. The water in a tissue is also not only free water, but a significant part of tissue water will be bound as a solvent shell to proteins, ions, and metabolic products. This bonding results in the inside of cells showing behaviour akin to gelatine. The cell membranes act both as a restriction, completely eliminating the movement of certain coupled water molecules through them, and as a hindrance, slowing the movement of water through them. All the above restrictions result in the diffusion coefficient of water being two-to-ten times lower in tissue than in an unrestricted medium [9].

The heterogeneity of the tissue is not random, biological systems have several levels of order to them. The easiest way to model this order is to imagine a system of tubes. These are densely packed, but do not touch each other. Inside the tubes, water can very easily diffuse along their axis, but will meet a restriction when moving to the tube wall. Outside the tubes, water can move around them, but suffers hindrance when diffusing towards or into the walls. This simple model can with some variance adequately represent the axons of neurons, with the water in the tubes representing intracellular water, and the compartment outside the tubes representing extracellular water.

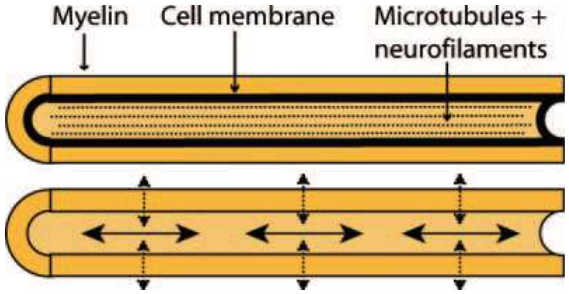

Figure IV.3: single-wall model of neurons, with added internal restriction via filaments [8]

Using the representation established in the previous section, we can visualize the diffusion in such a restricted system:

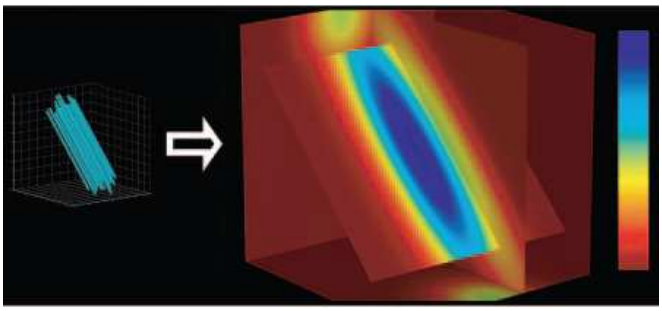

Figure IV.4: Diffusion with one axis of restriction [8]

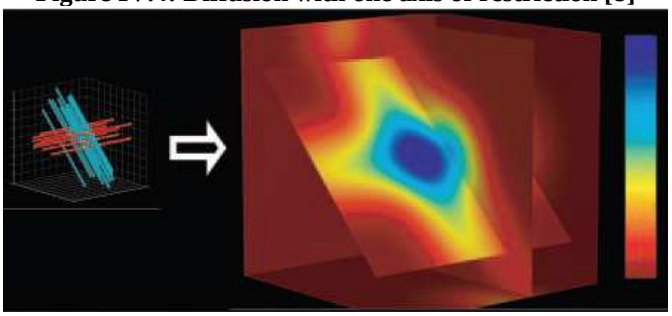

Figure IV.5: Diffusion with two restricted axii [8]

Figure IV.4 shows a diffusion profile with a single group of tubes, where there is a strong restriction in one direction, and none in the other directions, while Figure IV.5 shows the profile with two crossing tube groups, and the resulting restriction along two directions.

The aforementioned a model can be further refined by setting the walls as semi-permeable, in which case there is no absolute compartmentalisation of the water, and by setting the walls as non-permeable, in which case the system now contains two distinct water compartments. In reality, the tissue offers much more complex restrictive and hindering characteristics, with both intra and extracellular space containing many fibres, molecules, and tissue fragments that interact with free and bound water, and alter the diffusion profile.

The research of my diploma thesis pertains in part to distinguishing and verifying the various aspects of restriction and hindrance in MRI signal, both in vivo and in vitro.

IV.3: Diffusion-based imaging

In section IV.2, we showed that the heterogeneous nature of a tissue is represented in its diffusion profile. If we can image and map the diffusion profile, we can gather information about the heterogeneities. We can achieve this goal via diffusion based magnetic resonance imaging.

As described in the previous chapters, in MRI, all voxels can be assumed to have a different local magnetic field, and thus a different local resonance frequency. If a spin moves from one voxel to the next, it will experience a change in frequency, and therefore, a different phase. To describe this with a one-dimensional model, we must first quantify the change in the local field. We assume that the gradient of the field is linear in the investigated direction: $dG/dx=G$. If the movement speed is constant, then the spins movement is a random walk, and it can move δ distance in each $\varepsilon=\pm1$ step, needing τ time. Therefore, the field it experiences after n steps is [1]:

$$B(n\tau) = B(0) + G\delta\sum_{k=1}^{n}\varepsilon_k \tag{IV.5}$$

$$\Delta B(n\tau) = B(n\tau) - B(0) \tag{IV.6}$$

The phase change after one step is

$$\Delta\phi(\tau) = -\gamma\Delta B(\tau)\tau \tag{IV.7}$$

After N steps, it is:

$$\Delta\phi(N) = \sum_{k=1}^{n}\gamma\tau\Delta B(n\tau) = -G\delta\gamma\tau\sum_{k=1}^{N}\sum_{i=1}^{n}\varepsilon_i \tag{IV.8}$$

The longer the diffusion, the more phase change the spin suffers. If we consider not one spin, but a group of spins diffusing independently of each other, then the change is phase must lead to a loss of phase coherence. Using the central limit theorem, we can calculate that the mean square of the phase is:

$$\left\langle\Delta\phi^2\right\rangle = \frac{1}{3}G^2\gamma^2\delta^2N^3\tau^3/\tau \tag{IV.9}$$

Where $N^3\tau^3$ is the cube of the total time of the process, or t^3. It can be shown that a phase change leads to the following effect on magnetisation:

$$M_+ = M_0\exp\left(-\left\langle\Delta\phi^2\right\rangle/2\right) \tag{IV.10}$$

Combining the two equations above, as well as T_2 effects:

$$M_+(\text{diff.}) = M_0\exp\left(-G^2\gamma^2\delta^2N^3\tau^3/6\tau\right)\exp\left(-t/T_2\right) \tag{IV.11}$$

In a one-dimensional discreet model, the diffusion coefficient can be described with $D=\delta^2/2\tau$, leading to the following simplification:

$$M_+(\text{diff.}) = M_0\exp\left(-bD\right)\exp\left(-t/T_2\right) \tag{IV.12}$$

Here, b is used to denote:

$$b = -G^2\gamma^2 t^3 / 3$$
$$[b] = s / mm^2 \qquad \text{(IV.13)}$$

The three dimensional case can be described by the same term. If we only consider the diffusion term, then the change of magnetisation can be described as a loss of signal, since our spin packets suffer a net loss of phase coherence. This signal loss can be used to quantify the diffusion parameters of the investigated area.

Previously, we assumed that the gradient the spins experienced arose from simple motion. To investigate motion along a certain direction, a gradient must be introduced along that direction. This can be done in a gradient echo sequence, or in a spin echo sequence. Since the spin echo sequence is the easiest to visualise, we will use it as an example. The SE based diffusion sequence was first proposed by Stejskal and Tanner in 1965 [10], giving it its name. Real life pulse sequences have many more parameters and complexity, but the idea behind all of them is the same. Similarly, the exact parameters of the b-value vary with the sequences.

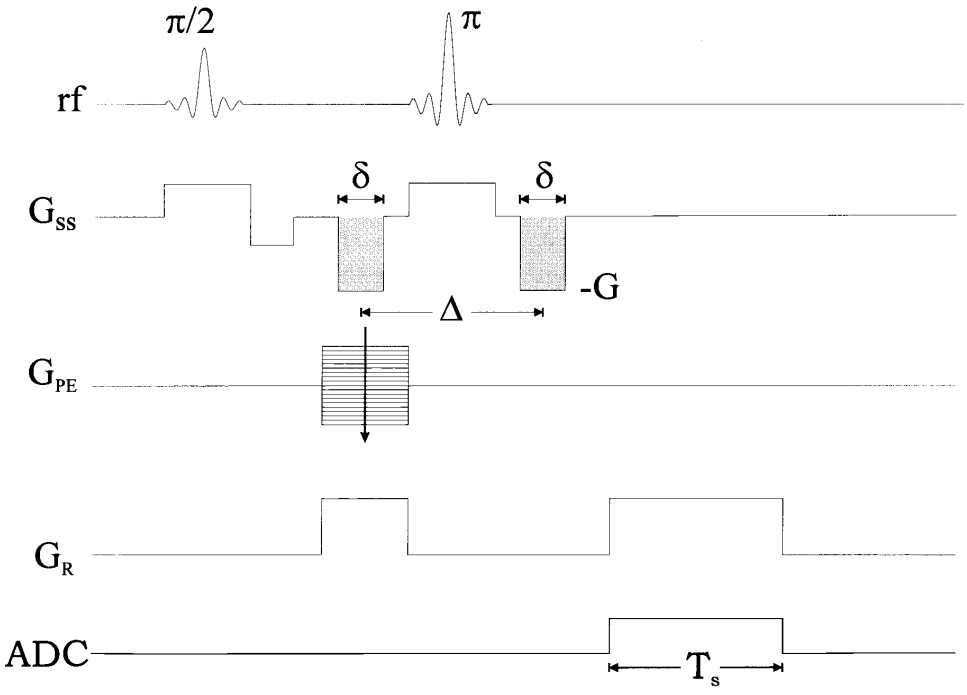

Figure IV.6: The Stejskal-Tanner spin echo sequence [1]

The sequence differs from a simple EPI spin echo sequence by the addition of the diffusion gradients, here incorporated into the slice select gradients. At t=0, the first diffusion gradient is applied for a δ time. This leads to a phase change that is dependent on the gradient strength, and therefore, the position of the excited spins. Second, a 180^o radiofrequency excitation is applied, which reverts the change in phase caused by the first gradient. Third, at t=Δ time, another diffusion gradient is applied, resulting in a phase change similar to the first. After this sequence, spins that have not moved from the investigated voxel have experienced a diffusion-induced phase-shift, a phase-inversion, and a shift on the inverted phase. The net result is a shift of zero. However, if a spin has moved, then the first and second gradients it experienced were different, leading to a different shift the first and the second time. The net result is a net shift in phase. Due to this shift in phase, there is a loss of phase coherence in the spin packet of the voxel, thus a loss of signal. The stronger the diffusion along the gradient, the higher the distance travelled during the Δ time period, and the higher the difference in phase shift at t=0 and t=Δ, resulting in a higher net loss of signal. For the Stejskal-Tanner pulse sequence, the b value is given as [10]:

$$b = -G^2\gamma^2\delta^2\left(\Delta - \delta/3\right) \qquad \text{(IV.14)}$$

It is evident, that the loss of signal is in itself not sufficient information. The loss of signal must be compared to the situation without applied diffusion gradients, or in other words, a b value of zero. Assuming the signal behaves exponentially with b, in accordance with equation IV.12:

$$I_S = I_0 \exp(-bADC) \qquad \text{(IV.15)}$$

Where I_S is the signal intensity measured with the diffusion gradients applied, and ADC is the apparent diffusion coefficient. The change of the signal intensity due to the applied diffusion gradients is therefore. This signal is the diffusion-weighted signal:

$$S = I_S/I_0 = \exp(-bADC) \qquad \text{(IV.16)}$$

S can only have values between one and zero. All other values are considered noise.

As previously described, the structure of an anisotropic medium is reflected in the diffusion profile. Thus any change is the structure can be mapped by measuring the diffusivity of water in the structure. This connection serves as the foundation of the medical use of diffusion imaging. Several diseases lead to changes in the microstructure of neuronal tissue, and these can be investigated in a diagnostic manner via diffusion imaging. [11]

To get complex structural information by measuring diffusion, more than one direction has to be measured. This is done by applying gradients in different directions.. Using one, or few diffusion directions in the basis of the diffusion-weighted imaging (DWI) method.

Let us assume that we have a restriction in our imaged system. We retain the Gaussian nature of the diffusion, but we apply a restriction, or anisotropy in certain directions, as shown on Figure IV.4. For each direction, the value of the diffusion coefficient can be measured, and from these values, the diffusion tensor can be constructed. Methods that require a diffusion tensor to be calculated are called diffusion tensor imaging (DTI). A tensor describing a restricted gaussian function is a diagonal 3-by-3 matrix. This matrix will have six independent elements, necessitating the measurement of at least six independent directions. From the measured and calculated ADC values, we can compile the diffusion tensor as generalized towards the principal axes.

$$\overline{D} = \begin{pmatrix} D_{xx} & D_{xy} & D_{xz} \\ D_{xy} & D_{yy} & D_{yz} \\ D_{xz} & D_{yz} & D_{zz} \end{pmatrix} \tag{IV.18}$$

Using the diffusion tensor, a simple quantifier of the diffusion strength, the mean diffusivity can be derived by taking the trace of the tensor. Calculating the eigenvalues gives us more information. Diffusion along any given direction can be described by the eigenvalues of the diffusion tensor:

$$\overline{D} = E^{T} \begin{pmatrix} \lambda_1 & 0 & 0 \\ 0 & \lambda_2 & 0 \\ 0 & 0 & \lambda_3 \end{pmatrix} E \tag{IV.19}$$

These eigenvalues represent the three largest diffusion coefficients. Due to the convention of matrix transformations, the above step can be understood as transforming the original Cartesian coordinate system of x,y,z into one of λ_1 λ_2 $\lambda 3$ [12]. Using them, the diffusion displacement probabilities can be easily visualised either as an isosurface, or as a directional probability surface:

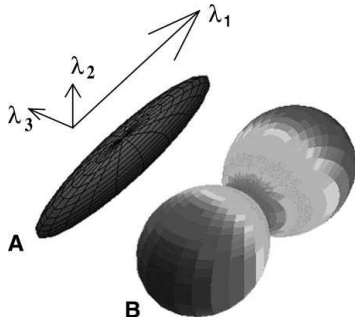

Figure IV. 7: For top to bottom: Eigenvalues of a diffusion tensor; A: isosurface representation; B: direction probability representation

The eigenvalues represent the anisotropy of the system, with the direction and size of the eigenvalues representing from the least restrictive direction to the most restrictive one. Using the eigenvalues, we can measure the anisotropy distribution of a given area, denoted as fractional anisotropy, or FA:

$$\mathrm{FA} = \sqrt{\frac{3}{2}} \sqrt{\frac{\left(\lambda_1 - \langle\lambda\rangle\right)^2 + \left(\lambda_2 - \langle\lambda\rangle\right)^2 + \left(\lambda_3 - \langle\lambda\rangle\right)^2}{{\lambda_1}^2 + {\lambda_2}^2 + {\lambda_3}^2}} \qquad \text{(IV.20)}$$

Fractional anisotropy is a number form zero, denoting isotropy to one, denoting total anisotropy, or in other words, a single diffusion direction. If a volume has a highly ordered structure with a distinct direction, it will have a high FA. A set of highly ordered structures in the same direction is a connection of these structures. Such a structure is, for example, a bundle of axons. Thus, FA maps give us very good information about the interconnectivity of the brain. Since there are many connections, it is useful to colour code them, by coloring the largest eigenvectors orientation: red denotes left-right, green shows anterior-posterior, and blue shows superior-inferior:

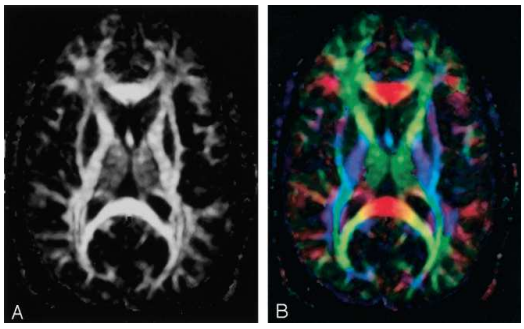

Figure IV.8: FA and colour coded FA [11]

Chapter V: b-dependent signal behaviour

In the normal clinical practice, diffusion measurements are usually carried out using a single b-value in the range of 800-1200 s/mm^2. This corresponds to an ADC about 10^{-3}mm^2/s, which is the diffusion speed of slightly restricted water in tissue. Higher b values are more sensitive for lower ADCs, and thus slower diffusion. Measurements with one b value conform to exponential signal behaviour, as described in equation IV.15.

However, measurements with multiple b values can reveal a different behaviour. In a non-restrictive medium, where the diffusion probability is equally distributed along each axis, the signal is still a monoexponential function of b. However, in restrictive structures,low and high b values lead to a different behaviour, that can be described by the following equation [13]:

$$S = f_{slow} \exp(-bADC_{slow}) + f_{fast} \exp(-bADC_{fast}) \qquad (V.1)$$

ADC_{slow} and ADC_{fast} are the apparent diffusion coefficients of the slow and fast signal components, while f_{slow} and f_{fast} represent the contribution of these components, with $f_{fast}+f_{slow}=1$. Describing the signal as two components description carries in itself the assumption that the signal arises from two compartments, and that there is little exchange between these two compartments.

In general, the two components are associated with the intra and extracellular water volumes of neuronal tissue. Measurements performed in rat brains resulted in $ADC_{fast}=(8.24\pm0.30)x10^{-4}$ mm^2/s, and $ADC_{slow}=(1.68\pm0.1)x10^{-4}$mm^2/sec, with $f_{fast}=0.8\pm0.02$, and $f_{slow}=0.17\pm0.02$ [14]. Measurements in human brains confirmed the approximate values of the rat brain ADCs and compartment weights [15].The fast ADC corresponds to the ADC measurable with a single b value in the 800-1200s/mm^2 range. Since extracellular water diffuses more freely, it is assumed that the majority of the signal in single-b measurements comes from extracellular water. The average compartmentalization of neuronal tissue is however 80% intracellular and 20% extracellular volume. [15]. This discrepancy between the signal compartments and the volume compartments questions the assumption.

In a complex medium, the compartment weights are related to the anisotropy of the medium. In the human brain, the more anisotropic white matter shows more prevalent biexponential signal behaviour, while the less ordered grey matter has small $f_{slow.}$ An isotropic medium shows exponential behaviour, with no distinct slow compartment.

Measurements conducted in [13] reveal the difference in behaviour:

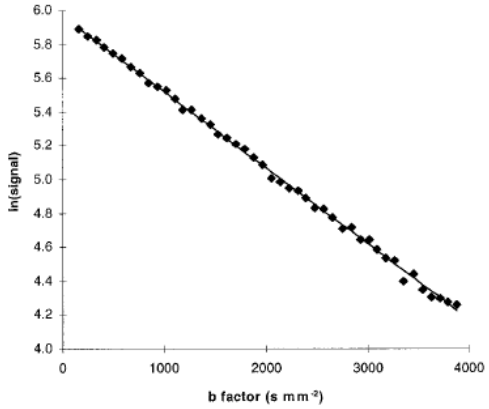

Figure V.1: Signal behaviour in isopropanol

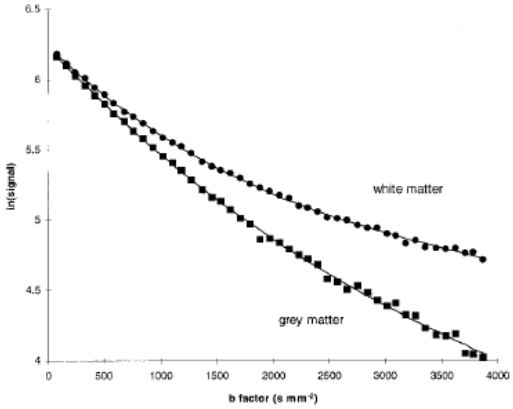

Figure V.2: Signal behaviour in grey and white matter

As evidenced by Figures V.1 and V.2, there is a strong correlation between the anisotropy of the signal and the anisotropy of the sample. Both figure are linear plots with regards to b, and natural logarithmic plots with regards to the signal. The logarithm of equation IV.15 is a linear function. As seen on Figure V.1, an isotropic sample, e.g. a vial of isopropanol, the plot is linear, thus the signal behaviour is monoexponential. Figure V.2 shows non-linear (thus biexponential) plots both for grey and white matter with the plot for white matter being much less linear than that of grey matter. This corresponds to the structural differences, as exlplained above..

Embedded in equation V.1 is an assumption of two water compartments that do not exchange spins with each other during the measurement. Equation V.1 is not theoretically calculated, but a best fit approach to data obtained by multiple b value measurements. As such, there are numerous proposals to alter the equation and the assumption embedded therein.

A histological investigation of white matter reveals not two, but three different and well-separated compartments: the extracellular space, the intracellular space, and the myelin sheaths separating the two. Based on this assumption, a model can be constructed [16].

The three compartments are absolutely separated, the permeability of each separating wall is set to zero. In this case, the intracellular water compartment impose strong restrictions due to its small size. Since restrictions are modelled with wall interactions, there will be monoexponential diffusion along the axis of the axon. Perpendicular to the axis, a Monte-Carlo simulation of such a model reveals a two-component signal behaviour, with only one of them (the extracellular)dependant on b:

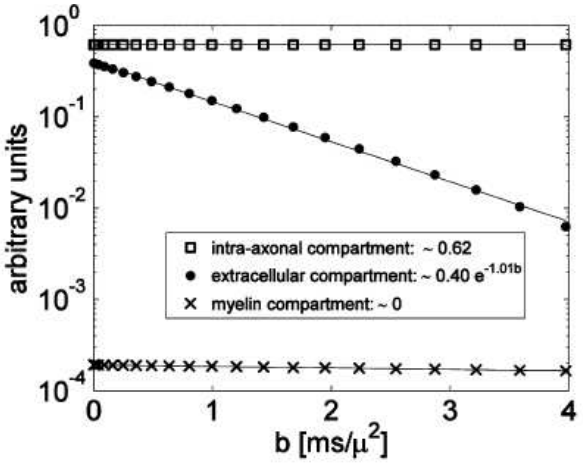

Figure V.3: MC simulation in [16], [ms/μ^2]=1000[s/mm^2]

The myelin component contains spins in a fatty, gelatinous medium, resulting in a very fast T_2 relaxation that overpowers the signal loss from diffusion, leading to no signal contribution. The intracellular component does not depend on b, while the extracellular component depends only monoexponentially on b. This model had been validated using formalin-fixed primate brains.

It should be noted, however, that [16] is based on the assumption that diffusion is Gaussian, hence the exponential behaviour. Thus, a non-exponential model can reject such an assumption, e.g. he signal can be modeled as a power series of b [17]:

$$\ln S = C_0 + C_1 b + C_2 b^2 + C_3 b^3 + ... \qquad (V.2)$$

This mathematically derived interpretation of the signal is independent of model assumptions. Tthe authors found that the using only baseline, b, and b^2 coefficients, the function fits well to data obtained in the b range of 50-2500 s/mm^2:

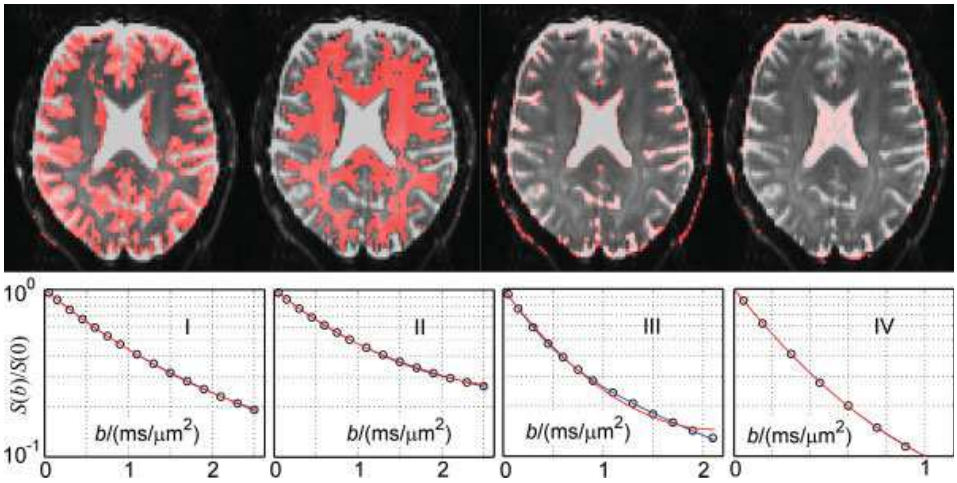

Figure V.4: **Fitting methods for ROIs shown in red [17]**

It should be noted, however, that this is exactly the range where the monoexponetinal fit is usually considered to be sufficient. [17]

The assumption most connected to my thesis is that two signal components can arise in a single compartment, as well. Single-cell diffusion measurements give information about the very basic processes underlying diffusion imaging. Such measurements were conducted on squid giant axons, lamprey spinal chords, and oocytes of Xenopus genera frogs [18,19]. The results of these studies show strong signal contribution of intracellular water, and non-monoexponential signal behaviour intracellularly. These studies, however do not necessarily reveal the basis of such signal behaviour. Even a single squid axon is a complex medium, with many intracellular bodies, e.g. membranes, mitochondria's, metabolic products and the cytoskeleton. Moreover, the diameters of the studied single cells (40-1000μm) are much bigger than that of a typical human axon (10μm). Therefore, the interpretation of results from theses studies is confounded by the significant size difference.

A more basic model requires the elimination of these internal and size-based obstacles. A 2003 paper [20] aimed to reduce the model to its absolute minimum, that of a single volume bordered by non-permeable walls. Thus, there is a single compartment without any internal restrictions, and any signal behaviour arises only from spin-spin and spin-wall interactions.

The volume can also be made to be dimensionless. The characteristic non-restricted diffusion length can be described as:

$$l_{char} = \sqrt{ADC \cdot \Delta} \qquad (V.3)$$

If the system has a size of l, the a dimensionless scalar can describe the ratio of the diffusion distance and the compartment size:

$$\alpha = l_{char}/l = \sqrt{ADC \cdot \Delta}/l \qquad (V.4)$$

In an ideal Stejskal-Tanner pulse sequence, the diffusion-weighted Bloch equations, which are the generalised form of the Bloch equations containing equation IV.11, can be solved analytically. The transverse magnetisation is then dependent on distances from the edge of the system. Intuitively, this can be described by seeing the centre of the system, where the edges are far, as a non-restrictive volume, where free diffusion can be used to describe the diffusion profile. Near to the edges, the spins will have their profile restricted, since diffusing in the direction of the edge, they will interact with the edge, bouncing of it. This behaviour is best described by the magnitude of said transverse magnatisation $|\sigma|$. The exact solution to the Bloch equations is dependent on the pulse forms. If in equation IV.14 , $\Delta=\delta$, the result is referred as Spin Echo, or SE in [20], while $\delta << \Delta$ is referred as the narrow pulse estimate, NP.

In [20], two models are considered. A one-dimensional model with a compartment size of 2a, and a two dimensional cylinder. The gradient was perpendicular to the boundaries in both cases, and b was fixed so that $bD_0=1$, where D_0 is the unrestricted diffusion coefficient. The results are as follows:

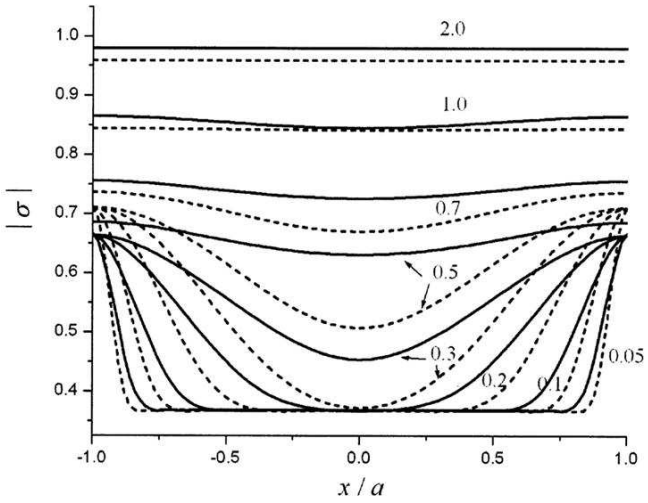

a_0/a	ζ		D_1		D_2	
	SE	NP	SE	NP	SE	NP
0.3	0.121	0.109	0.114	0.206	0.801	0.844
0.25	0.122	0.106	0.151	0.236	0.849	0.880
0.2	0.110	0.095	0.175	0.257	0.890	0.912
0.15	0.090	0.078	0.193	0.272	0.924	0.939
0.1	0.064	0.055	0.207	0.284	0.954	0.962
0.05	0.034	0.029	0.218	0.294	0.979	0.982
0.02	0.014	0.012	0.222	0.299	0.992	0.993

Figure V.5: Transverse magnetisation and diffusion coefficients obtained in a one dimensional model [20]

Figure V.5 shows the behaviour of transverse magnetisation as a function of the position in the system (x/α) at different α values in the SE (solid) and NP (dotted) estimations. As can be observed, once the diffusion distance and the compartment size are comparable,

that is, α>1, the edge effect starts to arise. With the decrease of alpha, the difference between magnetisation along the boundaries and in the middle increases sharply. This difference in magnetisation leads to a change in the local signal. The average signal for the whole compartment can be described as:

$$S = \zeta \exp(-bD_1) + (1-\zeta)\exp(-bD_2) \qquad \text{(V.5)}$$

The values of the parameters for equation V.5 are shown in the table on the right side of Figure V.5. The contribution of the slow (D_1) and fast (D_2) compartments is heavily dependent on α.

Results for a two dimensional cylindrical model are similar. Here, the volume can be described by the radial distance parameter of *p*. Figure V.6 shows the same dependence structure as Figure V.5:

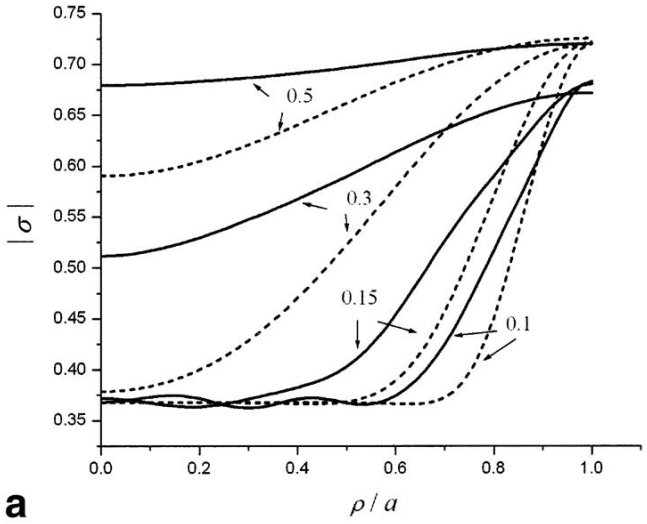

Figure V.6: Transverse magnetisation as a function of compartment size in a 2D cylinder [20]

At small α, the centre of the cylinder displays uniform magnetisation much lower than the edge, with a steep increase between the two regions. As the value of α increases, the difference between the two regions diminishes, and at α>0.5, the difference in negligible, with the whole cylinder displaying the same magnetisation. The resulting biexponential signal has been verified in experiments by Milne and Condradi [21].

NMR tubes of 160 μm and 50 μm inner radii were used in a 4.7T NMR machine at Oxford. NMR machines have the ability to measure very small samples in a very homogeneous magnetic field, and thus the result of [21] is only dependent on the compartment sizes, and the diffusion pulse parameters. With a δ of 3.0 ms and Δ of 54 ms for the 50 μm cylinder and 138 ms for the 160 μm cylinder, the ratio of the characteristic diffusion length and the compartment, defined as $\alpha = \sqrt{D_0 \Delta}/r$ was 0.2 for the smaller

cylinder and 0.1 for the larger. Measurements of the perpendicular diffusion signal capable of interacting with the barriers were conducted:

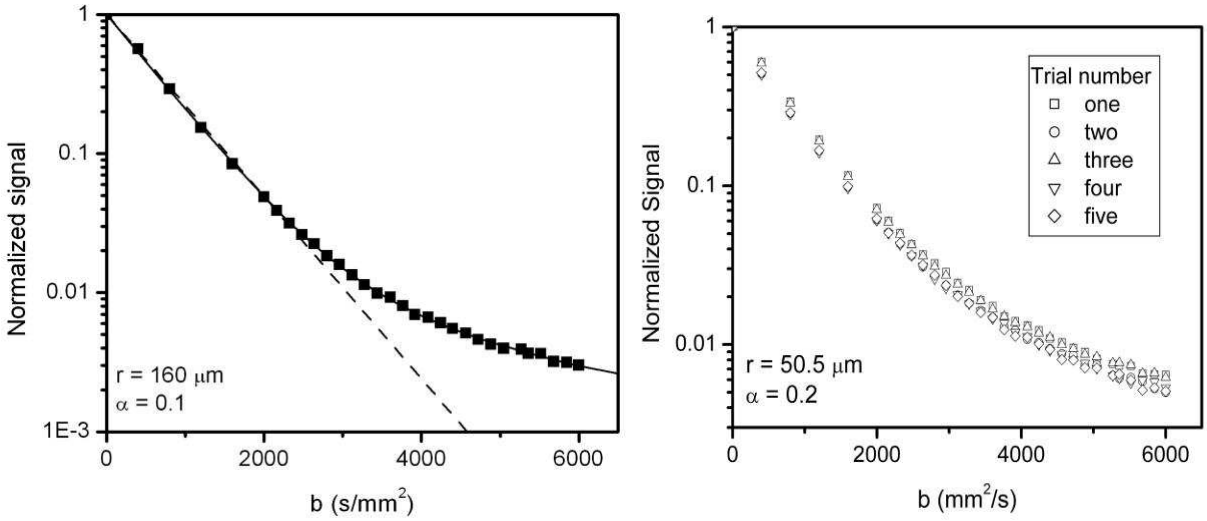

Figure V.7: experimental proof for biexponential signals in a single compartment system [21]

Figure V.7 shows the signal behaviour on a logarithmic scale in both tubes. It is evident from the data that the signal behaviour in not monoexponenetial, and that the data from the b range of 0-2500s/mm^2 shows a monoexponential behaviour in the form of the dotted line on the left. The cumulative contribution of the monoexponential part of the signal is in both cases more than 95%, meaning that the amount of spins carrying signal in the biexponential behaviour range is low.

Such a biexponential nature does not arise on the signal obtained by measuring the diffusion signal along the long axis of the cylinders:

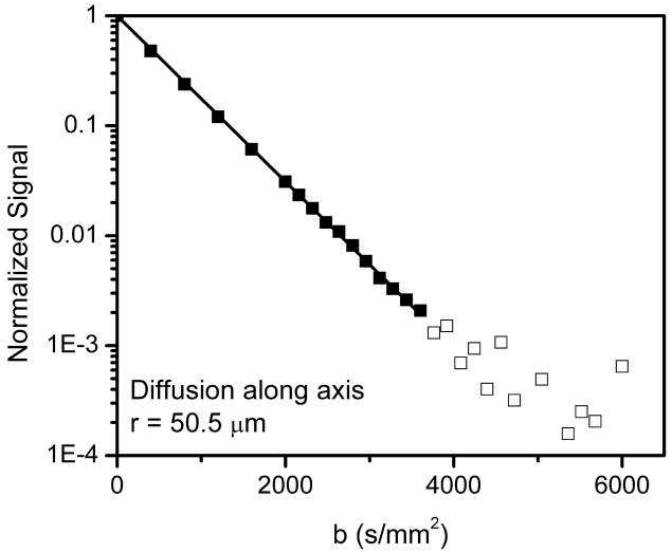

Figure V.8: Monoexponential diffusion along the axis [21]

The spins described by Figure V.8 did not encounter any boundaries along the long axis, therefore their diffusion is free and monoexponential.

Based on [20] and [21], we wanted to test the behaviour of the signal in a clinical scanner. [20] and [21] only pertain towards microscopic structures where the diffusion length and the compartment size are comparable. We wanted to test is this effect arises under circumstances where the compartment is many orders of a magnitude bigger than the diffusion distance. The papers discussed above only discuss a single distinct compartment. We wanted to test how the signal behaves in a set of many distinct single volume compartments, that can be understood to represent axon bundles.

We also tested the volumetric association described in [18] and [19] with a simple medium that contained only two water compartments.

To verify the clinical use of such measurements and data, we conducted a multi-b measurement on one healthy volunteer.

The results of our experiments are detailed in the chapters below.

Chapter VI: b-dependent diffusion signal intensity and fractional anisotropy in the human brain

VI:1: Fractional anisotropy as a function of b

The clinically used b-value discussed in chapters IV and V, ranging from 800 to 1200 s/mm^2, is based on practical considerations. For most clinical applications, such as the identification of tumours and changes in brain structure, such b-values are considered to be sufficient.

There are studies, however, that show better results, starker contrast in cases of brain infraction [22] and hepatocellular lesions [23], as well as increased sensitivity for detecting pancreatic adenocarcinomas [24].

Based on these results, we conducted an experiment on one healthy volunteer (26 y.o male). The volunteer had a pre-existing degeneration in his motor cortex, but was otherwise healthy.

Measurements were performed at the 3T Philliphs Achivea scanner of the Magnetic Resonance Research Centre (MRRC) of the Semmelweis University of Budapest, using an 8 channel SENSE head coil. Diffusion was measured along 32 non-collinear, independent directions in accordance with the recommendations of Derek Jones [25]. We measured the diffusion using eight b values: 800 s/mm^2; 1200 s/mm^2; 1600 s/mm^2; 2400 s/mm^2; 3200 s/mm^2, 4000 s/mm^2, 4400 s/mm^2 and 4800 s/mm^2. The field of view was 240·240·140 mm, voxel size was 2·2·2 mm.

Data was exported from the scanner in DICOM format, then converted to N1fTI using MRICron [26]. These NIFTI files were analysed by using the FDT diffusion toolbox of FSL [27], following the common pipeline for the process [27]. Eddy current correction was performed on all images, as was brain extraction. Fractional anisotropy maps were created using the dfit tool. NIFTI images and fractional anisotropy (FA) maps were converted to MATLAB [28] matrices and later analysed that format.

We analyzed fractional anisotropy maps in three transverse planes along the z direction. These planes were: z=50 mm; z=70 mm, and z=90 mm.

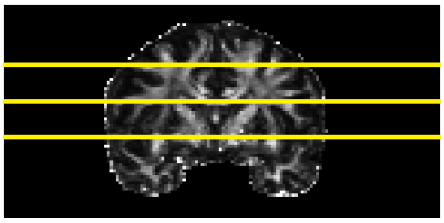

Figure VI.1:The three planes of investigation

In the transversal plane z=50 mm, the fractional anisotropy images were the following:

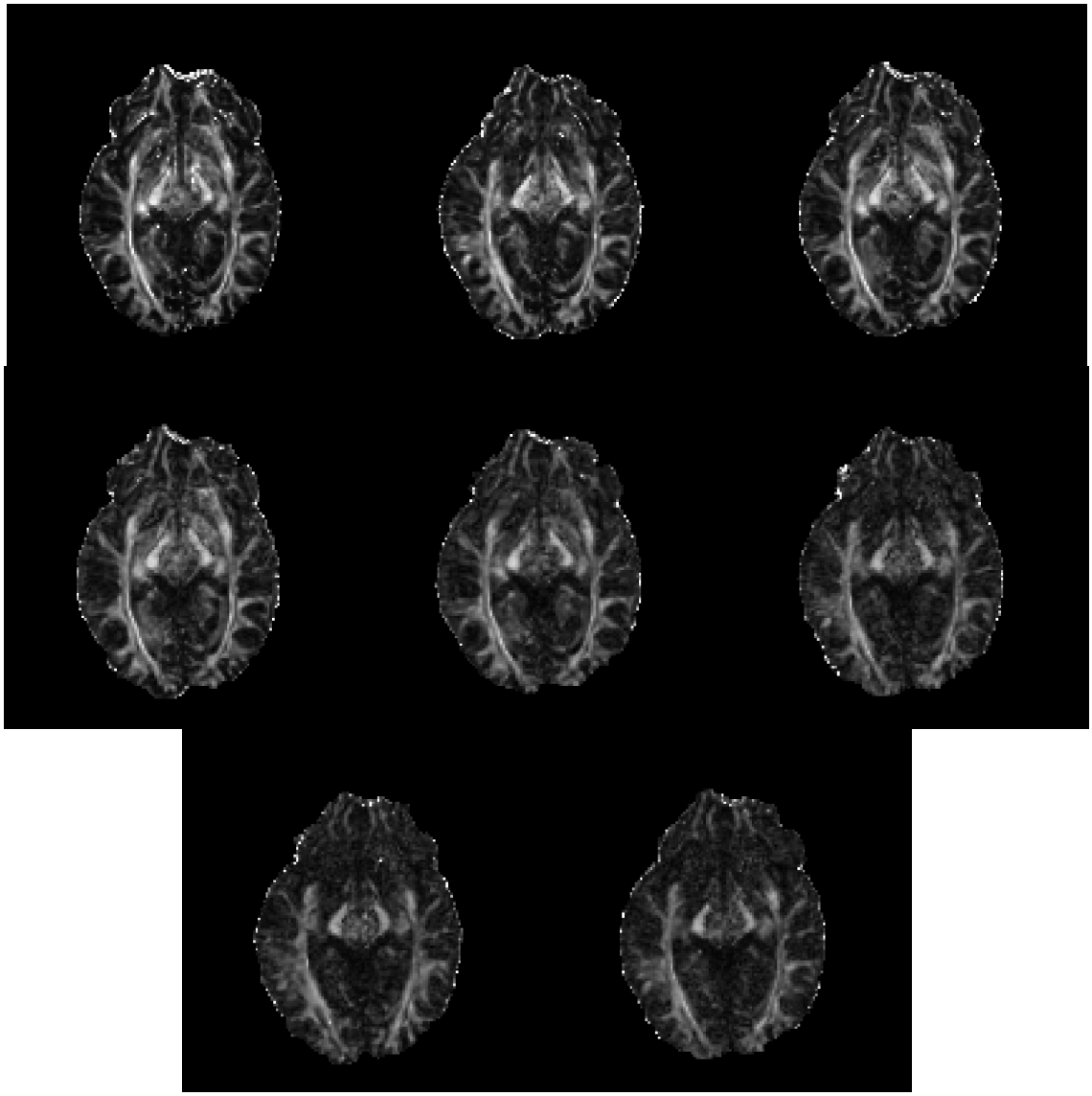

Figure VI.2:Fractional anisotropy maps for transversal plane z=50 mm at b values of 800 (top left); 1200 (top middle), 1600 (top right); 2400 (centre left); 3200 (centre middle); 4000 (centre right); 4400 (bottom left); and 4800 (bottom right)

Figure VI.2 shows that the fractional anisotropy diminishes with higher b values. The stark contrast of the first map is greatly reduced by b=4800 s/mm^2. The clearly visible connections between the anterior and posterior parts of the brain on the images taken with low b values cannot be seen on the maps taken with higher b values. The noise level increases

sharply with b. While on the first maps, the posterior medial part shows clear connections with high contrast, on high b values, the area is indiscernible from noise.

A visual inspection of the FA maps does not show the difference in fractional anisotropy as such. To analyze the difference, we calculated the difference between the maps corresponding to higher b values, and the map of b=800 s/mm2. These difference maps are show on Figure VI.3. The high difference values resulting from either the brain outline or not complete overlap, classified as absolute differences higher than 0.8 were removed. All images are greyscale images scaled from -1 (black) to +1 (white).

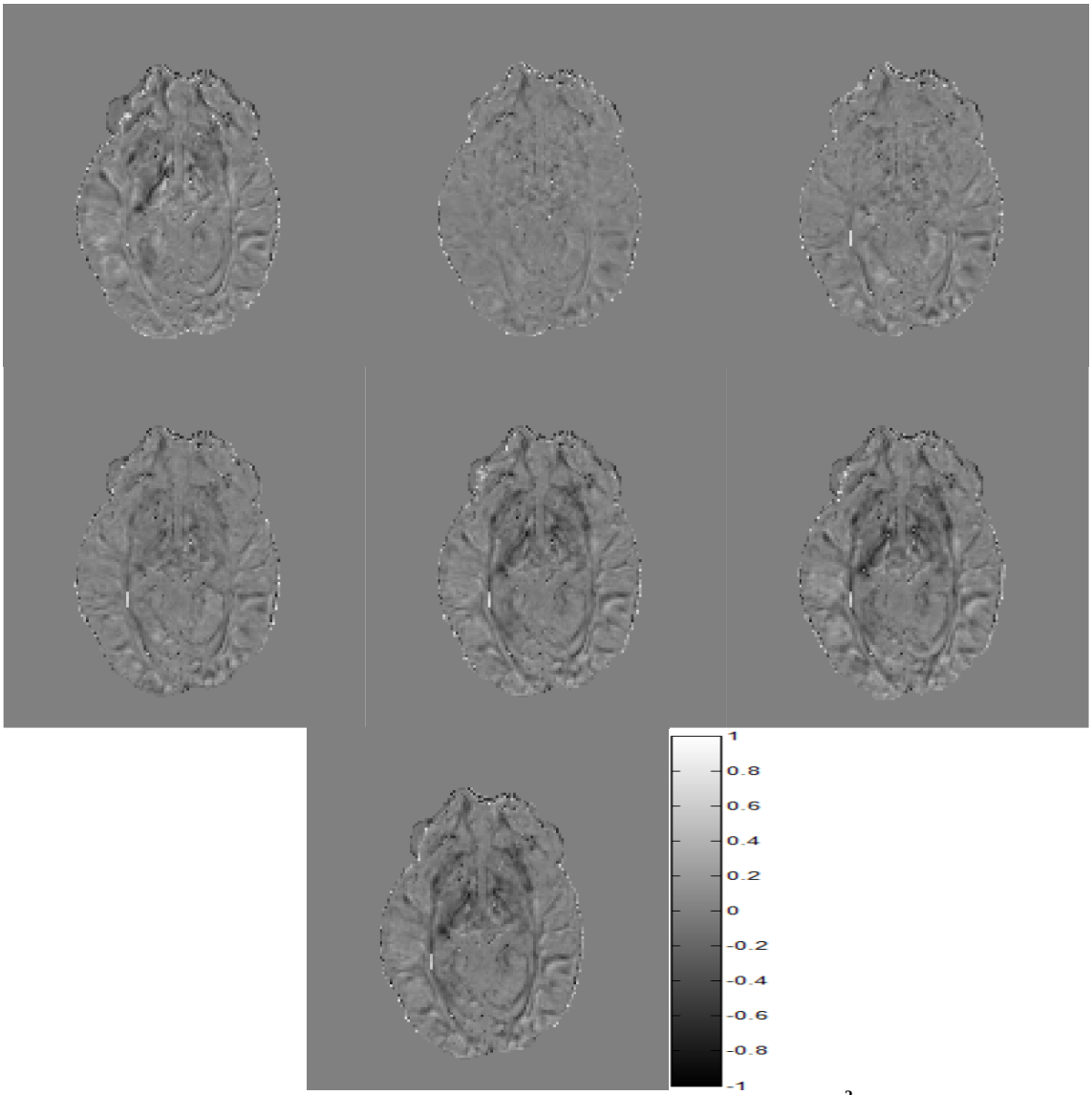

Figure VI.3: Fractional anisotropy difference maps compared to b=800 s/mm^2,for transversal plane z=50 mm
at b 1200 (top left); 1600 (top middle), 2400 (top right); 3200 (centre left); 4000 (centre middle); 4400 (centre right); and 4800 (bottom right)

As seen of Figure VI.3, at all b values, the difference in the anterior-posterior connections are evident. At high b values, the dorsal-ventral connections show a marked

difference compared to the base image if 800 s/mm^2. There is very little ordered difference between 800 s/mm^2 and 1600 s/mm^2, while both 1200 and 2400 show a difference.

We quantified the difference using three parameters. The average to the negative value differences (k_{neg}), which shows the average FA decrease due to the change of b. The average of positive values (k_{pos}) shows the FA increase, while the average taken over the whole FA range (k_{avg}) shows a net difference in the contrast.

b value of the compared image [s/mm^2]	k_{neg}	k_{pos}	k_{avg}
1200	-0.0184	0.0152	-0.0032
1600	-0.0099	0.0099	-0.0001
2400	-0.0130	0.0118	-0.0012
3200	-0.0191	0.0090	-0.0100
4000	-0.0258	0.0102	-0.0156
4400	-0.0293	0.0110	-0.0183
4800	-0.0285	0.0087	-0.0198

Table VI.1:Differences in FA at z=50 mm

The differences shown indicate that the FA of higher b images is always lower, and thus, averaged over the whole of the image, more difficult to discern. A visual inspection of the FA maps also shows that very high b value measurements do not return enough information about connectivity. The visual and numerical differences between FA maps taken with 800 s/mm2 and those taken with 1200 s/mm^2 or 1600 s/mm^2 is, however not that pronounced.

For z=70 mm and z=90 mm planes, only the differences and their numerical quantifications are shown.

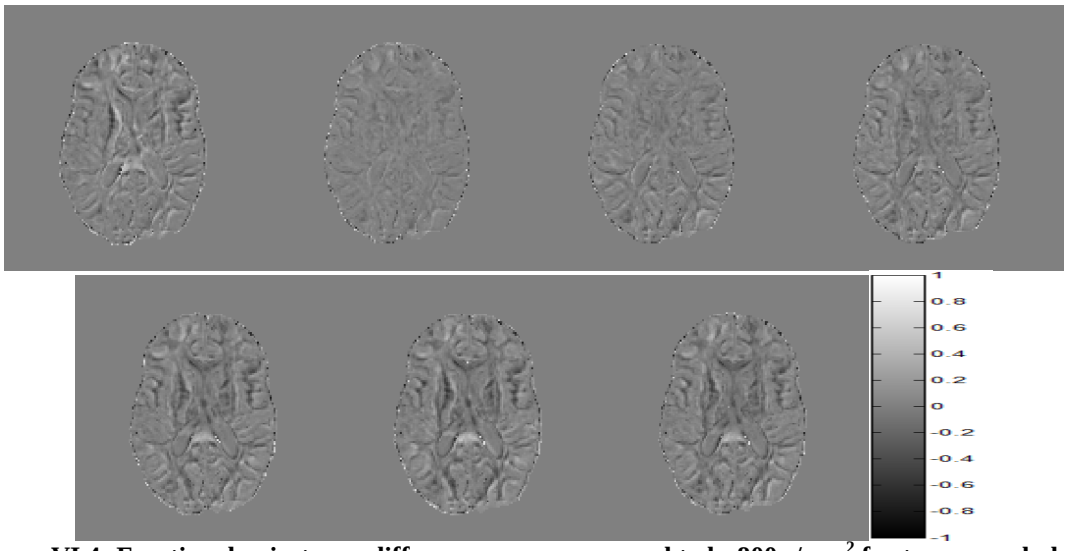

Figure VI.4: Fractional anisotropy difference maps compared to b=800 s/mm^2,for transversal plane z=70 mm
at b 1200 (top far left); 1600 (top left), 2400 (top right); 3200 (top far right) ; 4000 (bottom left); 4400 (bottom centre); and 4800 (bottom right)

b value of the compared image [s/mm^2]	k_{neg}	k_{pos}	k_{avg}
1200	-0.0145	0.0179	0.0033
1600	-0.009	0.0095	0.0006
2400	-0.0125	0.0106	-0.0019
3200	-0.0148	0.012	-0.0028
4000	-0.0194	0.0148	-0.0046
4400	-0.0213	0.0161	-0.0051
4800	-0.0208	0.014	-0.0068

Table VI.2: Quantified differences in FA at z=70 mm

Table VI.2 shows that on the lower b values, the difference is less marked, as discussed above. The positive total FA difference in the first two values means that an this plane, it would be beneficial to measure fractional anisotropy with b values 1200 s/mm^2 or 1600 s/mm^2, but the effect of incomplete brain outline and noise removal can not be discounted.

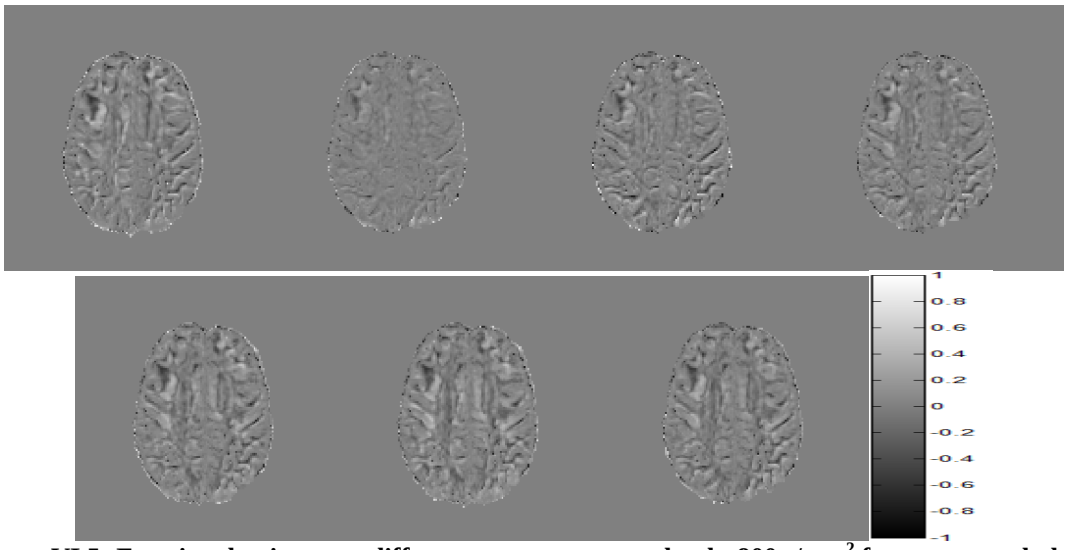

Figure VI.5: Fractional anisotropy difference maps compared to b=800 s/mm^2,for transversal plane z=90 mm
at b 1200 (top far left); 1600 (top left), 2400 (top right); 3200 (top far right) ; 4000 (bottom left); 4400 (bottom centre); and 4800 (bottom right)

b value of the compared image [s/mm^2]	k_{neg}	k_{pos}	k_{avg}
1200	-0.0132	0.0186	0.0054
1600	-0.0081	0.0093	0.0012
2400	-0.0114	0.0116	0.0002
3200	-0.0129	0.0132	0.0004
4000	-0.0138	0.0182	0.0044
4400	-0.0143	0.0197	0.0054
4800	-0.0151	0.0154	0.0003

Table VI.3: Quantified differences in FA at z=70 mm

The average difference is positive, even if very low. Based on these three planes, we suggest that 1200 s/mm^2 and 1600 s/mm^2 might be feasible b values for measuring fractional anisotropy. However, the differences are not very pronounced, and ultimately, the choice must always be with the referring physician and/or the medical physicists performing the scan.

VI.2: Diffusion signal in the brain

Diffusion signal intensity was also investigated. We selected three regions on interest, each of 3×3×3 voxels, characterizing very dissimilar areas of the brain. The third ventricle as a mainly fluid region, the corpus callosum as a white matter region, and the visual cortex as a mainly grey matter region. All diffusion weighted images were corrected for nonperfect coregistration and noise by removing voxels with signal intensities higher than one.

Due to the complex nature of the brain, this method is very susceptible to the region of interest selection. Due to this sensitivity, we did not perform a numerical analysis of the data, and we only show the signal behaviour.

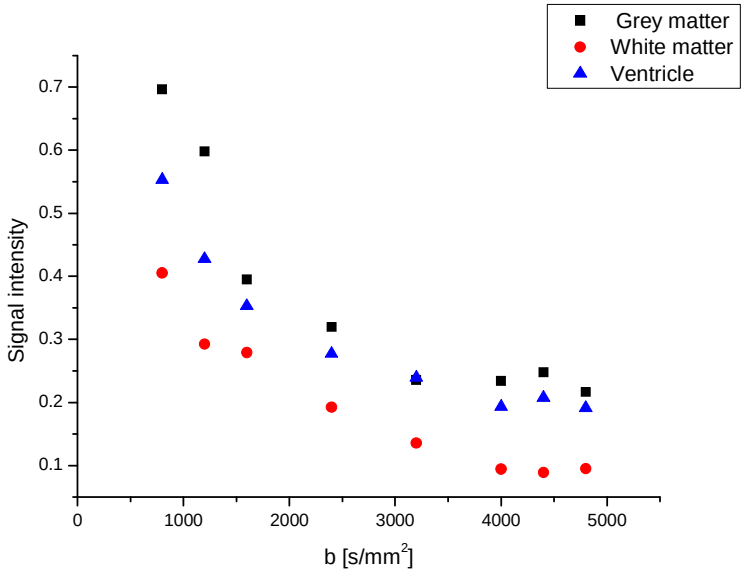

Figure VI.6: Signal intensity in the three different ROIs of the brain

As can be seen, white matter is the most restrictive structure of the investigated ROIs. Grey matter and the ventricle have a similar diffusion profile. This is probably due to liquor pulsation in the ventricles. The investigated region of grey matter is also very rich in sulci and gyri (highly gyrificated), leading to a significant signal distortion. In all cases, the signal diminishes with the increase of the b value, though a clear mono or biexponential nature can

not be discerned. Plotting the natural logarithm of the signal gives more information. The natural logaritm of a monoexponential signal is linear, while in a biexponential, this is not true.

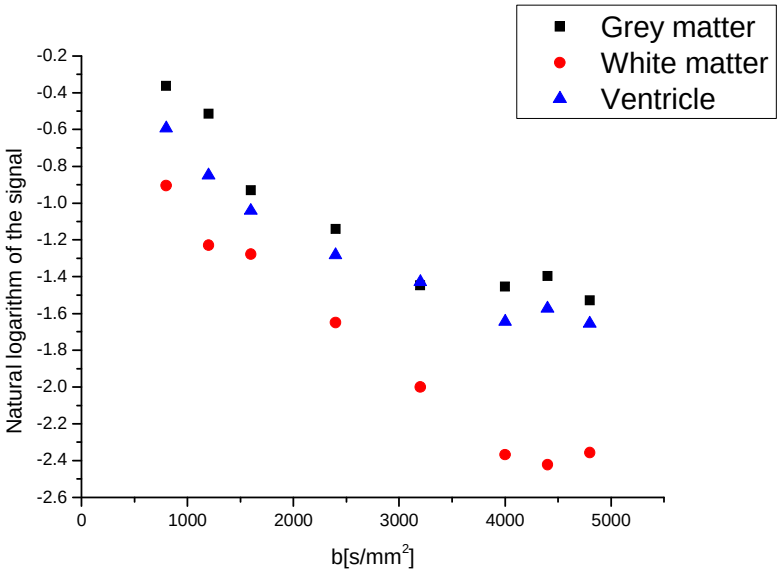

Figure VI.7: Natural logarithm of the signal in the ROIs

There is no clear linear characteristic for any of the three ROI. The difference between grey and white matter becomes more evident on the graph above. Based on this observation, we concluded that in this measurement with this scanner, all investigated parts of the brain, and by projection, the brain as a whole, shows a non monoexponential diffusion profile.

Chapter VII: b-dependent diffusion signal intensity measurements in compartment phantoms

As described in Chapter V, non-monoexponential signal behaviour can arise from factors other than volumetric association. Specifically, biexponential signal behaviour has been shown in single compartment systems where the diffusion distance is comparable to the size of the compartment.

We wanted to investigate if this effect can be measured in the clinical scanner of the MR Research Centre, and if this effect can also arise in a macroscopic phantom.

VII.1: Measurements in a macroscopic phantom

Based on the results of [21], we wanted to measure whether barrier effects arise if the compartment is not in the same size scale as the diffusion distance. Even so, with the voxel sizes typical in clinical applications, a voxel close to an impermeable barrier may contain a different diffusion profile, since the restricted particles very close to the barrier can interact with the particles in the voxel, and this may lead to a change in the signal.

For this measurement, we used a beaker of 6.5 cm diameter, filled with distilled water. Water, glass, and air have significantly different magnetic susceptibility values, therefore we placed the above beaker into a bigger one of 9.5 cm diameter, also filled with distilled water. Our original beaker was thus far from the air-water border, and did not suffer from significant susceptibility artefacts.

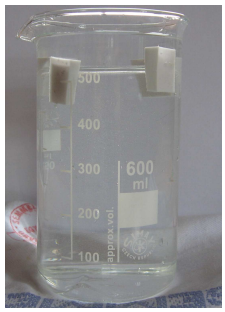

Figure VII.1: The macroscopic phantom

We used b values from 200 s/mm2 to 5000 s/mm2, with an increment of 200 s/mm2 per step. Our field of view was 256·256·70 mm, with voxel sizes 2·2·2 mm. Diffusion was measured in the directions x;y;z;-x;-y;-z. The measurements along the negative axes were done to minimise the effect of gradient field and radiofrequency field inhomogeneities. Each

measurement was repeated three times, leading to 18 measurements for each b value. The orientation was such that the z direction was parallel to the long axis of the beaker.

Data was exported to DICOM files, and converted to NIFTI, and analysed with MATLAB and OriginPro software.

We analysed three distinct volumes. Two volumes of 5×5×5 voxels; the centre of the beaker, where, according to our hypothesis, there should be monoexponential diffusion, and a volume close to the edge of the beaker, where we might expect to find a change in the signal behaviour. For each direction and its opposite, we averaged the signals of the six measurements.

Figure VII.2 shows the signal intensity as a function of the b value in the two volumes, along three directions:

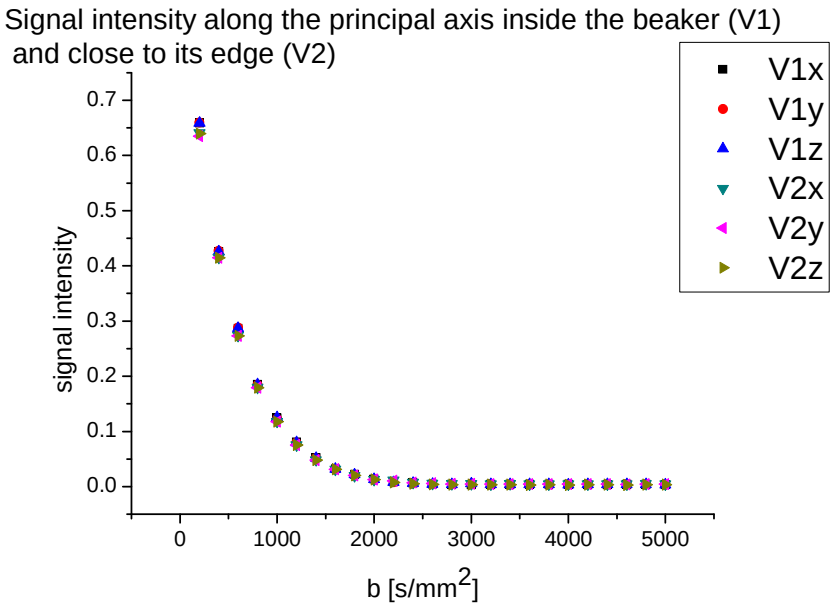

Figure VII.2: Signal intensity in two volumes of the beaker

In figure VII.2,V_1 denotes the volume in the centre of the beaker, far from the walls, while V_2 denotes the volume closer to them. The figure shows exponential signal behaviour in all directions and in both volumes. This behaviour was analyzed by fitting both monoexponential and biexponential curves onto the data points. The monoexponential fit function was $y=A\cdot\exp(-b\cdot x)$; the biexponential fit function was $y=A\cdot\exp(-b\cdot x)+(1-A)\cdot\exp(-c\cdot x)$. The starting parameters for iteration of the biexponential fit were the results of the monoexponential fit. Fitting was performed with the Matlab curve fitting tool.

Monoexponential fit						
	V_{1x}	V_{1y}	V_{1z}	V_{2x}	V_{2y}	V_{2z}
A	0.9998	1	1.001	0.9802	0.9705	0.9788
bounds of A	0.9877, 1.012	0.9872, 1.013	0.9884, 1.014	0.9705, 0.99	0.9612, 0.9798	0.9692, 0.9884
b	0.002104	0.002104	0.002107	0.002131	0.002121	0.002134
bounds of B	0.002075, 0.002133	00204, 0.002135	0.002077, 0.002138	0.002107, 0.002155	0.002099, 0.002144	0.00211, 0.002157
r^2	0.9997	0.9997	0.9997	0.9997	0.9997	0.9997
Biexponential fit						
A	0.9614	0.9796	0.9625	0.9215	0.8349	0.9576
bounds of A	-4.312, 3.0356	-3.9345, 2.0423	-3.9648, 3.1845	0.8942, 1.231	0.7534, 1.4234	0.7593, 1.156
b	0.002125	0.002108	0.002124	0.002268	0.002355	0.00225
bounds of b	0.0007095, 0.00354	0.0005565, 0.009782	0.0005161, 0.003732	0.001915, 0.002622	0.001683, 0.003026	0.002063, 0.002437
c	0.001666	0.001896	0.00168	0.001369	0.001541	0.001133
bounds of c	-0.02378, 0.02711	-0.3183, 0.3221	-0.02849, 0.03185	-0.00074, 0.003478	-0.000383, 0.003464	-0.0005541, 0.002821
r^2	0.9997	0.9997	0.9997	0.9997	0.9997	0.9997

Table VII.1: Biexponential MATLAB curve fitting results for the two volumes and three direction

While both the mono, as the biexponential fits result in good r^2 values, denoting well fitting curves, the confidence intervals for A, or the intensity distribution ratio are far greater if the biexponential fit is applied to the internal volume (V_1), where we assume monoexponential signal. Apparent diffusion coefficients for both volumes and both fitting methods are close to 10^{-3} mm^2/s, i.e. the diffusion coefficient of free water. The diffusion coefficient for the signal component of lower intensity (parameter c) is in all cases significantly lower, about half the coefficient of the high intensity component. In case of the V_2 volume, this could be a result of restricted diffusion arising from the closeness of a restrictive barrier in the form of the edge of the beaker.

Since monoexponential curves could be fitted with good confidence intervals to both volumes, we performed further analysis with another method. The natural logarithm of a monoexponential function is a linear function, while that of a biexponential function is not. Therefore, is we plot the signal intensities with respect to b, we should see if a certain signal is monoexponential or not.

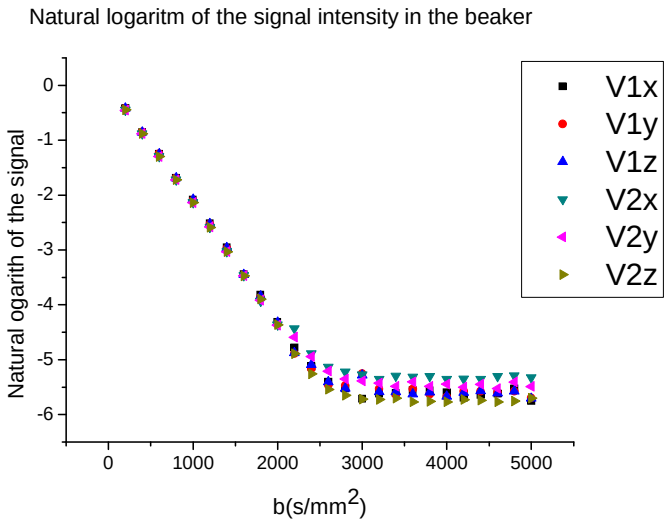

Figure VII.3: The natural logarithm of the signal in figure VII.2

Figure () shows that the natural logarithms of the measured signals are not linear functions of b, thus these signals are not completely monoexponential. This is true for both investigated volumes, possibly due to impurities of water used in the experiment. However, in the range of 2200 s/mm^2 or higher b values, there is a difference in signal intensities between the centre volume, most prominent in the x directional signals (the direction in which volume 2 was closest to the wall of the beaker). This means that despite the possible impurities, or other effects causing non-monoexponential behaviour globally, there is still an effect arising from one volume being close to the wall, or the edge of the compartment:

:

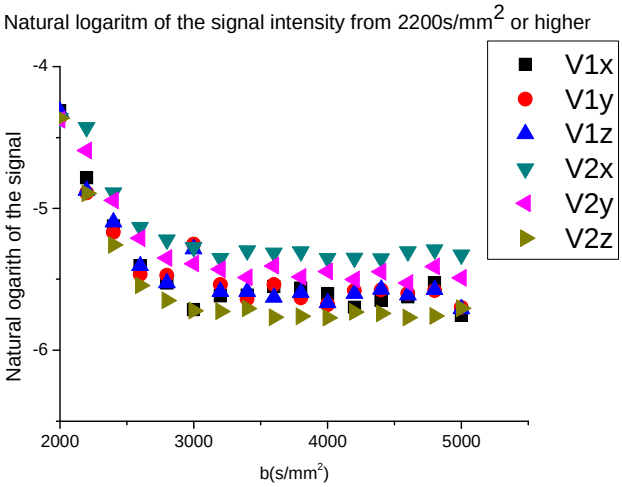

Figure VII.4: The b>2000 s/mm^2 part of figure VII.3

The difference shown on figure VII.4 can be quantified in the following way. The signal intensity measured along the x direction, the direction where the volume was closes to the wall, was compared for each b value to the averaged signal intensity of the V_1 volume:

b [s/mm^2]	Signal difference [%]
2200	9
2400	5
2600	5
2800	5
3000	3
3200	4
3400	6
3600	5
3800	5
4000	5
4200	5
4400	4
4600	5
4800	5
5000	7

Table VII.2: Signal difference in the x direction

Table VII.2 shows a signal difference of 2-9%. This signal difference is probably caused by the voxels closest to the edge of the beaker, where the diffusion profile is severely distorted by the presence of an impermeable wall. This distortion is very prevalent on voxels that are just one voxel away from the wall. Voxels directly adjacent to the wall were not taken into consideration to avoid partial volume effects. Figure () shows two example voxels, vox_x, close to the barrier along the x dimension, and vox_y, close to that barrier along the y dimension. In both cases, the graph shows the average signal intensity over all dimensions.

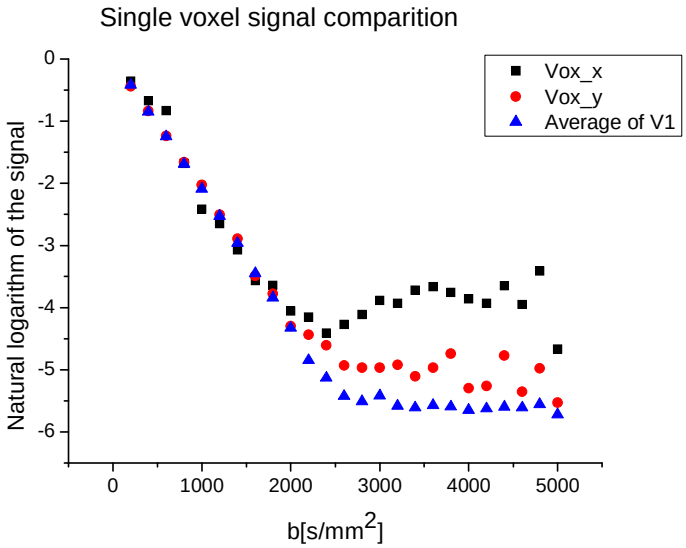

Figure VII.5: Signal intensity comparison for two near-barrier voxels and the middle sample

Even if only the averages of the single voxel signals are taken into consideration, the difference between the signals is statistically significant on b values of 2200s/mm^2 or higher ($p<0.001$) . The difference between the signal intensities in vox_x and vox_y, compared to the signal average of V_1:

b [s/mm^2]	Signal difference [%]	
	Vox_y	Vox_y
2200	14	8
2400	14	10
2600	21	9
2800	25	10
3000	28	8
3200	29	12
3400	33	9
3600	34	10
3800	33	15
4000	32	6
4200	30	6
4400	35	15
4600	30	5
4800	37	10
5000	18	3

Table VII.3: Signal difference for single, near-barrier voxels

Based on these results, we conclude that, when measuring diffusion with in the clinical scanner of the MRRC in a macroscopic, non.restrictive medium, the signal will not show a completely monoexponetial behaviour. This non-monoexponentiality increases as the investigated volume is moved closer to the barrier of the medium. The non-monoexponential part is significant above b values of 2200s/mm^2. Voxels very close to the barrier contribute to this part of the signal if the investigated volume is close to the barrier. Averaging over many voxels, some closer to the barrier than others, diminshes the effect of the wall.

VII.2: Measurements in test tubes and capillaries

Based on our results discussed above, we wished to investigate the signal behaviour in more constrained volumes. To this end, we constructed a set of phantoms using laboratory test tubes of 0.75 cm diameter, filled with capillaries of 150 μm diamater. Three phantom were used. Two tubes filled with capillaries and distilled water, resulting in a maximal radial compartments size in the x-y plane of 75 μm, and one test tube without capillaries, filled with distilled water. The capillaries were held in place by foam pads at both ends of the test tubes. During the measurements, the capillaries were put into a heat bath to keep them from warming.

Our measurements were conducted using the same scanner and coil as before. The field of view was 128·128·96 mm, with voxel size being 1·1·1 mm. Diffusion was measured along six directions, and repeated three times, like in the previous measurement. The b values

encompassed the range 800-4800 s/mm^2, with an increment of 400 s/mm^2. Diffusion signal intensity was investigated in 5·5·5 voxel volumes in each test sample. Orientation was such that the z axis corresponded to the long axis of the samples.

Data was first analyzed by taking the natural logarithm of the signals and plotting it against the b values:

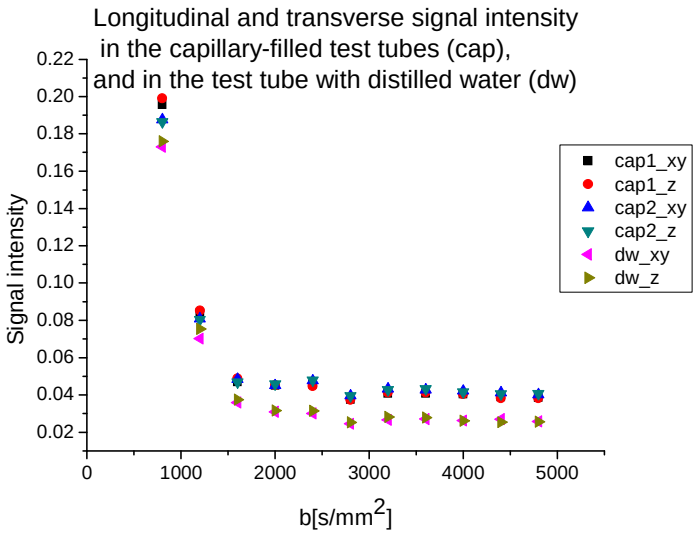

Figure VII.6: Longitudinal and transverse signal intensity for the three samples

Figure VII.6 shows a marked difference in the signal intensity for the two capillary-filled tubes and the test tube filled with distilled water (cap1, cap2, and dw respectively). The signal of the two test tubes filled with capillaries does not differ from each other greatly. For this reason, we calculated the average of the signals in the capillaries, and compared that to the signal of the test tube filled only with distilled water:

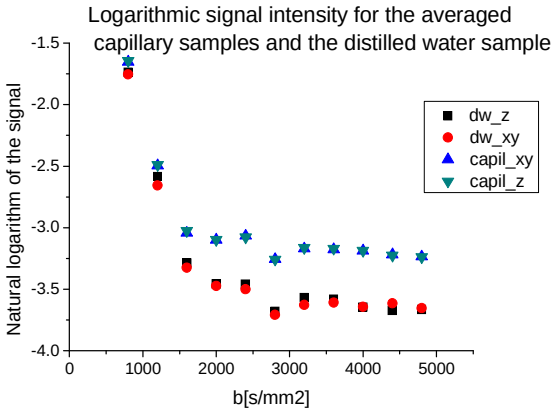

Figure VII.7: Averaged longitudinal and transverse signal intensity for the three samples

As seen of Figure VII.7, the signal is not completely monoexponential in either case. The difference from the monoexponential signal behaviour is greater in the samples filled with capillaries. There is a linear behaviour in the logarithmic signal for b values under

2000s/mm^2, therefore on those ranges, the signal behaves monoexponentially. The difference between the signals from the capillaries depends on the b value in the following way:

B values [s/mm2]	Signal difference in the x-y plane [%]	Signal difference along z axis [%]
800	10	9
1200	17	10
1600	32	29
2000	45	43
2400	54	46
2800	57	52
3200	58	50
3600	53	51
4000	57	58
4400	48	56
4800	52	53

Table VII.4: Signal intensity difference between the capillariy sample and the distilled water sample

As can be seen on Table VII.4, the difference in the signals is more than 50% on high b values. This can be interpreted as the effect of the much higher restriction in those test tubes that are filled with capillaries. The difference is much higher compared to the case of single voxel in the beaker. This is due to reduced distances to the edge of the compartment, which in the case of the capillary-filled test tubes, is smaller than the voxel.

Curve fitting based analysis was performed on the averaged data on the two tubes with capillaries and the test tube filled with distilled water.

Monoexponential fit				
	$capil_{xy}$	$capil_z$	dw_{xy}	dw_z
A	0.256	0.2611	0.4767	0.4581
bounds of A	0.09654, 0.4137	0.09878, 0.4235	0.112, 0.8415	0.1335, 0.7826
b	0.0006783	0.0006902	0.001372	0.001305
bounds of B	0.0002672, 0.001089	0.000275, 0.001105,	0.0006492, 0.002095	0.0006494, 0.00196
r^2	0.5982	0.6444	0.7869	0.7805
Biexponential fit				
	$capil_{xy}$	$capil_z$	dw_{xy}	dw_z
A	0.226	0.231	0.4558	0.4374
bounds of A	0.1968, 0.2555	0.2021, 0,2606	0.4439, 0.4676	0.4252, 0.4496
b	0.0009752	0.0009816	0.00161	0.001534
bounds of b	0.0004832, 0.001467	0.000497, 0.001466	0.001356, 0.001864	0.001285, 0.001783
c	0.0001323	0.0001058	0.00007176	0.0000235
bounds of c	0.000075634, 0.000213	0.0000348, 0.0002123	0.00000931, 0.000121	0.00000436, 0.00008676
r^2	0,7261	0,7317	0.9129	0.9144

Table VII.5: Curve fitting analysis of the signal in capillaries and distilled water samples

The very low values for the signal intensity in the monoexponential case are the result of a strong overall restriction. As can be derived from equation IV.16, a higher restriction leads to a lower intensity. For this reason, the buiexponential fit was modified in the following way: $y=A\cdot B\cdot\exp(-b\cdot x)+A\cdot(1-B)\cdot\exp(-c\cdot x)$, where B is the parameter deterimned by the fitting, and A is the intensity parameter of the monoexponential fit. Table () show the corrected (A·B) value. Both samples show strongly non-monoexponential signal behaviour, evidenced by the low r^2 values. In the capillary-filled test tubes, the apparent diffusion coefficients for both the mono and the biexponential fit are at least one magnitude lower than the diffusion coefficient of free water. This is due to the very tight restrictions caused by the capillaries.

In the distilled water filled test tube, the monoexponential fit shows an apparent diffusion coefficient close to the diffusion coefficient of free water. The biexponential fit show a very low diffusion coefficient for the slow signal component, which could be the result of thermal convection.

From these multiple analyses, we conclude that the non-monoexponential nature of the signal depends very strongly on the effective distance from the edges of the compartment. If the investigated volume is relatively far away from the barrier of the compartment, the apparent diffusion coefficient is comparable to that of free water. If the barrier is close in terms of diffusion distance, the signal is distorted by components of slow diffusion coefficients. If the compartments are small enough to fit multiple times into a single voxel, then this effect is greatly increased, and the diffusion coefficients are an order of a magnitude lower.

Chapter VIII: Measurement of volumetric signal association using red blood cells

As described in Chapter V, the signal components can be attributed to intracellular and extracellular volumes. While ratio of the signal components is not the same as the ratio of the volumes, changes should occur if the volume ratio is changed.

In our experiments, we aimed to demonstrate that this association is measurable in a clinical scanner, and can thus be important clinically, and that there is a correlation between the signal behaviour and the ratio of intra and extracellular water compartments.

To measure this effect, we had to find a viable sample. As a general rule, tissue contains more than just the cells and water surrounding them. Collagen fibres, macromolecules, and various other extracellular structures, while playing a part in the signal behaviour, are not associated with the volume of the sample, or the volume of the cells. For our measurements, we needed a tissue that with a great oversimplification is just intracellular water in the form of cells, and extracellular water in the form of a solution.

Red blood cells and saline solution fulfil these criteria. A mix of red blood cells and saline (henceforth referred to as saline solution), created from a blood pack, has only intracellular water in the form of the intracellular water of the red blood cells, and a negligible amount of white blood cells, while the extracellular water is only the solution. The red blood cells, when treated with anti-coagulation agents, will not form extracellular structures. Therefore, the cells will move around freely in the sample, and any restriction to diffusion will arise solely from the cells membranes separating the water into extra and intracellular compartments.

The ratio of the compartments can also be changed easily. Saline solution is isotonic with regards to red blood cells. Thus, if we dilute the sample, the red blood cells do not suffer swelling, so only the ratio of the intra-, and extracellular compartments changes.

We have obtained our samples from the Hungarian National Blood Transfusion Service. Two 250ml bags of red blood cell solution were supplied with a haematocrit fraction of 60%.

We conducted two sets of measurements, first a pilot to investigate the feasibility of measurements, and secondly a more detailed set with many ratios of intra and extracellular water.

VIII.1: Pilot measurement

Our first measurement was conducted with only one dilution step, thus only one change in the compartment ratio. We filled a beaker of 6.5 cm diameter with saline solution from one of the blood bags. This beaker was placed in the head coil, positioned to be in the central axis of the MR machine. The sample was previously kept in cold storage, thus it was left to reach thermal equilibrium with the environment. Temperature was monitored during the measurement, and it was found to be constantly 22±1 ^{o}C.

The following imaging parameters were used: field of view=96·96·70 mm; voxel size=1·1·1 mm. Diffusion was measured along six axes, x,y,z, and -x, -y, -z. The signal was measured at 12 b values, from, 200 s/mm^2 to 5000 s/mm^2 in incremental steps of 400 s/mm^2. Temperature measurements were performed after 1400 s/mm^2, 2600 s/mm^2 and 3800 s/mm^2. During each temperature measurement, the sample was stirred to prevent sedimentation.

The sample was afterwards diluted with 250 ml of isotonic saline, thus doubling the absolute volume, and decreasing the haematocrit fraction to 30%. Measurements were performed at five b values from 1000 s/mm^2 to 5000 s/mm^2, in increments of 1000 s/mm^2.

Data was extracted as DICOM files, converted to NIFTI format using MRIcron software, and converted to MATLAB data. Analysis was performed with MATLAB and Origin 8.

Diffusion signal intensity of both measurement sets, averaged for all six axes, and averaged for a 10×10×10 voxel volume in the middle of the sample is shown of figure VIII.1:

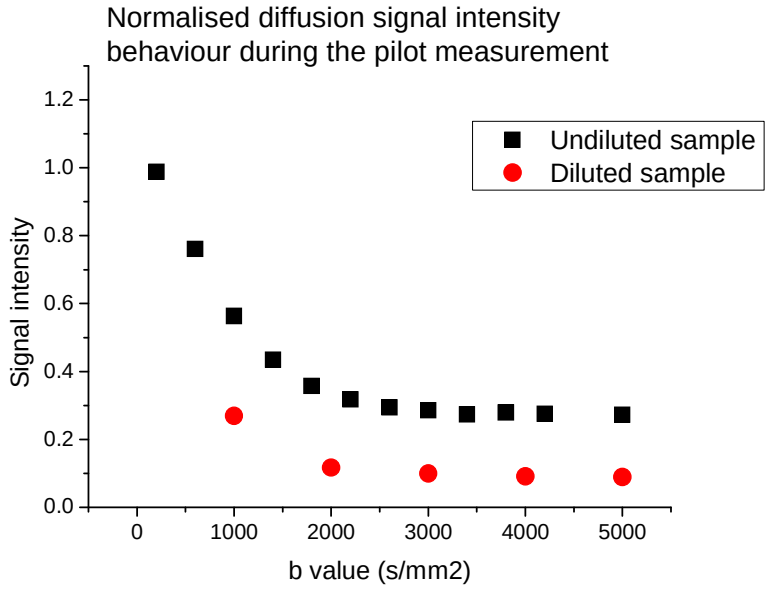

Figure VIII.1:Normalized signal intensity for diluted and undiluted red blood cell solution

As can be seen, the dilution caused a significant change in overall diffusion signal intensity. Since we only measured five points for the diluted sample, an analysis of biexponentiality was not feasible. However, based on the difference in intensity, we conducted measurements with more dilution factors.

VIII.2: Measurement with multiple dilutions

For our multiple dilution measurements, we used the second blood pack. Field of view and voxel size were the same as in the pilot measurement. Diffusion was again measured along six direction and the measurements was performed three times. B values rose from 500 s/mm^2 to 5000 s/mm^2, in increments of 500 s/mm^2. To prevent sedimentation, the sample was stirred after measurements with 1500 s/mm^2 and 3000 s/mm^2. The original, undiluted volume of 210 ml was diluted in steps to 320 ml, 420 ml, 500 ml and lastly 970 ml, leading to haematocrit values of 60%; 39%; 30%; 25%; 13% respectively. A 5×5×5 voxel volume in the middle of the sample was used for the analysis.

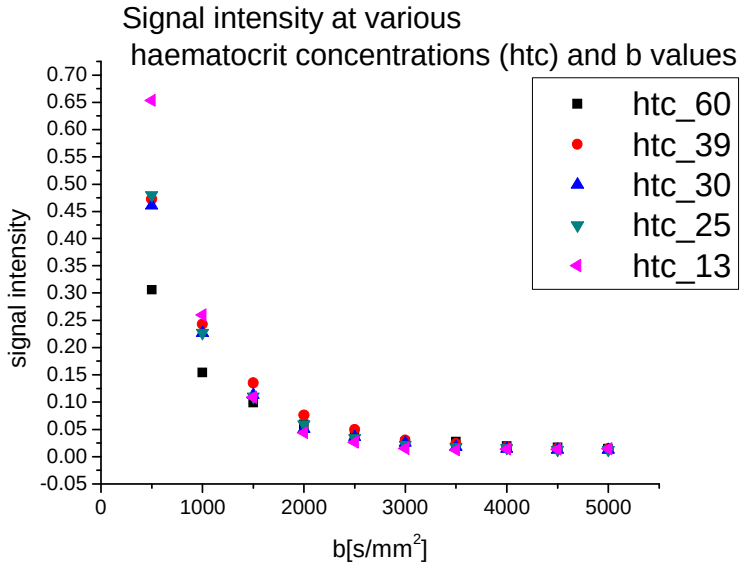

Figure VIII.2:Non-normalized signal intensity for multiple dilution factors

As seen on Figure VIII.2, the repeated measurement did not show a very marked difference in signal intensity between the various samples of different haematocrit concentrations. All signals behave in an exponential fashion. The natural logarithm of the signal was also analyzed.

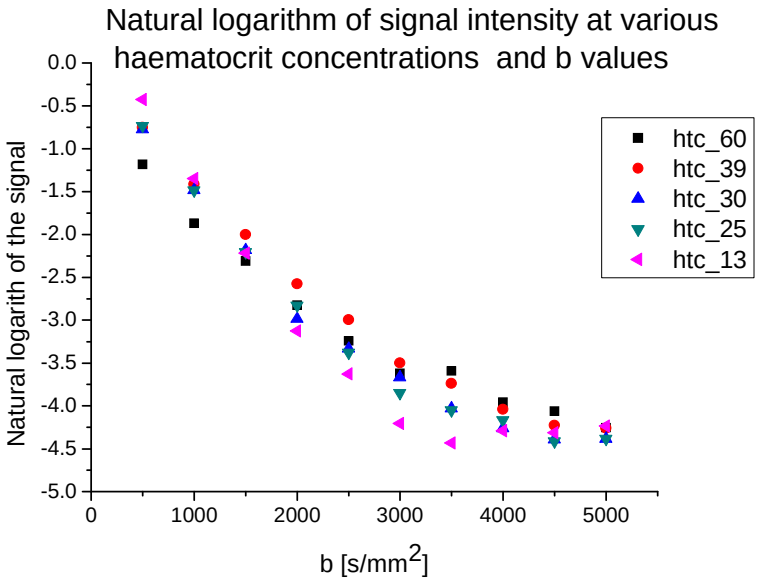

Figure VIII.3: Natural logarithm of signal intensity for multiple dilution factors

At all dilutions, the signals show a different behaviour than in the experiments with distilled water. There is no clear break in the logarithmic signal, and the linear part goes on to b=3000 s/mm^2. While a difference in signal behaviour is evident from the logarithmic figure, further analysis was performed via fitting curves onto the signal.

The biexponential fit was done in the following way: y=A·B·exp(-b·x)+A·(1-B)·exp(-c·x), where B is the parameter to be determined by the fitting, and A is the intensity parameter of the monoexponential fit. In table (), the corrected value is shown as A', while the calculated A·(1-B) value is shown as D'.

Monoexponential fit					
	60%	39%	30%	25%	13%
A	0.5074	0.8534	0.9138	0.9714	1
bounds of A	0.4286, 0.5863	0.7785, 0.9284	0.8306, 0.997	0.8841, 1.059	0.6342, 1.366
b	0.001075	0.001209	0.001379	0.001425	0.001231
bounds of b	0.0008981, 0.001252	0.0011, 0.001317	0.001258, 0.001501	0.001302, 0.001547	0.0007754, 0.001687
r^2	0.9819	0.9952	0.9958	0.9961	0.9438
Biexponential fit					
A'	0.4934	0.8415	0.9038	0.9612	0.9999
bounds of A'	0.4329, 0.5541	0.8046, 0.8781	0.8736, 0.9339	0.9386, 0.9843	0.9964, 1.003
D	0.01399	0.01186	0.00996	0.0102	0.00001
b	0.001166	0.001259	0.001425	0.001471	0.001231
bounds of b	0.0009461, 0.001386	0.001168, 0.00135	0.001339, 0.00151	0.001405, 0.001537	0.001132, 0.00133
c	0.0000103	0.0000103	0.0000105	0.000016	0.0001231
bounds of c	-0.0009959, 0.001016	-0.000737, 0.000757	-0.000731, 0.0007511	-0.0005494, 0.0005515	0.0001031, 0.0001343
r^2	0.9915	0.9984	0.9985	0.9993	0.9358

Table VIII.1: Curve fitting analysis of diffusion signal for multiple dilutions

From these results, we can see that the diffusion coefficient of the fast fraction, or the extracellular space is close to that of unrestricted diffusion, as we expected. The diffusion coefficients of the slow component are two orders of a magnitude lower, possibly denoting a connection between the measured slow component and the intracellular water. As can be seen in the last column, when the intracellular water component is only 13%, the biexponential fit becomes almost monoexponential, with the weight of the fast fraction very close to one.

The A and A' parameters, which denote the signal change due to diffusion, also correlate with the dilution. Since the higher this parameter is, the lower the signal change is, this behaviour is consistent with the theory. Lastly, the ratio of D and A', the parameters of the slow/fast signal components, can be investigated. This ratio is 2,83% for the undiluted sample, 1,41% for the first; 1,1% for the second, 1,06% for the third, and 0,001% for the fourth dilution. While this ratio is not consistent with the ratio of intra and extracellular water, it does change in accordance with the dilutions. The slow signal component is diminished as the ratio of intracellular water is lowered.

Sedimentation was measured in the most diluted sample by performing five scans of b=1000 s/mm^2 in sequence. This took 20 minutes. There is no marked difference between the signal intensities in either case, thus, the effect of sedimentation of the signal was ruled to be minimal.

Therefore, we conclude that there is a connection between biexponential signal behaviour and intra-, extracellular water compartmentalisation, and that this is measurable on clinical 3T scanners.

Chapter IX: Summary and conclusions

During the measurements for my master's thesis, we conducted diverse measurements pertaining to the signal intensity as a function of the b value, both in vivo and in vitro.

For imaging the human brain, different b values, thus different measured diffusion speeds were shown to lead to different fractional anisotropy maps. These maps were compared to each other numerically and visually. From the standpoint of a physician, the best maps were those measured at b values from 800 s/mm^2 to 2400 s/mm^2. Signal intensity was also compared in different regions of interest in the brain. Each region showed a non-monoexponential signal behaviour, and the signal behaviour was found to differ with the regions. From this we concluded that the structural makeup of the brain influences the signal behaviour, depending on the local structures.

We tested the hypothesis that non-monoexponential signals can arise in single compartment system. In a macroscopic phantom, the non-monoexponentiality of the signal was found to be stronger when measured in volumes close to the barrier of the compartment, and was very strong in single voxel measurements on the edge of the barrier.

This non-monoexponential behaviour was also found to arise in test-tube and capillary sized systems. In this comparison, we found that the capillary system, where the compartment length was orders of magnitude lower than in both the macroscopic phantom and the test tube, the non-monoexponential signal component was stronger.

We also conducted experiments regarding the volumetric association of the non-monoexponential signal. Using saline solution of red blood cells, we found that the signal intensity changes with the ratio of extra-, and intracellular water. The slow and fast signal component changes were found to correlate to the intra-, and extracellular volume changes.

From these measurements, we conclude, that in a 3T clinical scanner, in our experimental arrangements, a non-monoexponential diffusion signal can arise from both barrier effects in a single compartment, and volumetric association in a multi-compartment system.

Acknowledgements

I would like to express my gratitude to the people who have assisted me during the writing of this thesis. First and foremost, I would like to thank my supervisor, Lajos Rudolf Kozák, for his continued support during the writing and fine-tuning of this thesis. I thank his PhD student, Ádám Szabó, for the invaluable help he has lent me with data processing. I thank the operators of the MR Research Centre, and its director, professor Gábor Rudas, for letting me conduct my measurements.

I would like to thank Sándor Nagy, of the Hungarian National Blood Transfusion Service, for providing us with the blood sample.

I thank Gyula Kovács for introducing me to diffusion-weighted MRI, and in turn, Lajos Rudolf Kozák.

Without Kálmán Nagy, my teacher of MRI physics, I would not be writing this thesis.

I give my sincere thanks to Dávid Légrády, my supervisor from the Department of Nuclear Techniques, for his patience, and his help with overcoming bureaucratic hurdles.

Table of references

[1] E. MARK HAACKE et al: Magnetic *Resonance Imaging:Physical Principles and Sequence Design*; Wiley; 1998

[2] ZHI-PEI LIANG et al:, *Principles of Magnetic Resonance Imaging: A Signal Processing Perspective;* IEEE Press; 2000

[3] JOHN C. EDWARDS: *Principles of NMR*; http://www.process-nmr.com/nmr1.htm

[4] W. W. ORRISON et al: *Functional Brain Imaging*; Mosby; 1995

[5] E. L. HAHN: *Spin echoes*; Physical Review 80; 1950

[6] MR Safety Homepage: http://www.mrisafety.com/

[7] KAZUKO TANAKA: *Self-diffusion coefficients of water in pure water and in aqueous solutions of several electrolytes with ^{18}O and ^{2}H as tracers;* Journal of the Chemical Society, Faraday Transcripts 1; 1978

[8] PATRIC HAGMANN: *Understanding Diffusion MR Imaging Techniques: From Scalar Diffusion-weighted Imaging to Diffusion Tensor Imaging and Beyond***;** Radiographics 26; 2006

[9] DENIS LE BIHAN**:** *The 'wet mind': water and functional neuroimaging*; Physics in Medicine and Biology 52; 2007

[10] E.O. STEJSKAL, J.E. TANNER: *Spin Diffusion Measurements - Spin echoes in the presence of a time-dependent field gradient;* Journal of Chemical Physics 42; 1965.

[11] PETER J. BASSER; DEREK K. JONES: *Diffusion-tensor MRI: theory, experimental design and data analysis - a technical review*; NMR in Biomedicince 15; 2002

[12] BRIAN J. JELLISON et al*: Diffusion Tensor Imaging of Cerebral White Matter: A Pictorial Review of Physics, Fiber Tract Anatomy, and Tumor Imaging Patterns*; American Journal of Neuroradiology 25; 2004

[13] CHRIS A- CLARK, DENIS LE BIHAN: *Water Diffusion Compartmentation and Anisotropy at high b Values in the Human Brain*; Magnetic Resonance in Medicine 44; 2000

[14] NIENDORF et al: *Biexponential diffusion attenuation in various states of brain tissue: implications for diffusion-weighted imaging*. Magnetic Resonance in Medicine 36; 1996

[15] C. NICHOLSON, E. SYKOVA: *Extracellular space structure revealed by diffusion analysis*; Trends in Neuroscience 21; 1998

[16] SHARON PELED: *New perspective on the sources of white matter DTI signal;* IEEE Transactions On Medical Imaging 26; 2007

[17] V. KISELEV, K. ILYASOV: *Is the "biexponential diffusion" biexponential*; Magnetic Resonance in Medicice 57, 2007

[18] C BEAULIEU, PS. ALLEN: *Water diffusion in the giant axon squid: implication for diffusion-weighted MRI of the nervous system*; Magnetic Resonance In Medicine 32; 1994

[19] M. TAKAHASHI et al: *Magnetic resonance microimaging of intraaxonal water diffusion in live excised lamprey spinal cord*; Proceedings of the National Academy Of Sciences; 2006

[20] A. L. SUKSTANSKIJ, J.H.H ACKERMAN, D.A. YABLONSKIY: *Effects of Barrier-Induced Nuclear Spin Magnetisation Inhomogeneities on Diffusion-Attenuated MR Signal*; Magnetic Resonance In Medicine 50; 2003

[21] M. MILNE, M. CONRADI: *Mutli-exponential signal decay from diffusion in a single compartment*; Journal Of Magnetic Resonance; 2009

[22] JR. MEYER et al: *High-b-value Diffusion-weighted MR Imaging of Suspected Brain Infarction;* American Journal Of Neuroradiology 21; 2000

[23] F. AGNELLO et al: *High-b-Value Diffusion-weighted MR Imaging of Benign Hepatocellular Lesions: Quantitative and Qualitative Analysis*; Radiology; 2012

[24] T. ICHIKAWA et al: *High–b Value Diffusion-Weighted MRI for Detecting Pancreatic Adenocarcinoma: Preliminary Results;* American Journal Of Radiology, 2007

[25] D.K. JONES et al:*Optimal strategies for measuring diffusion in anisotropic systems by magnetic resonance imaging*; Magnetic Resonance In Medicine; 1999

[26] MRIcron homepage: http://www.mccauslandcenter.sc.edu/mricro/mricron/

[27] FSL homepage: http://www.fmrib.ox.ac.uk/fsl/

[28] MATLAB homepage: http://www.mathworks.com/products/matlab/

[29] Origin Pro homepage: http://www.originlab.com/